Enhancement of snow albedo reduction and radiative forcing due to coated black carbon in snow

Wei Pu[1], Tenglong Shi[1], Jiecan Cui[1], Yang Chen[1], Yue Zhou[1], Xin Wang[1,2]

[1]Key Laboratory for Semi-Arid Climate Change of the Ministry of Education, College of Atmospheric Sciences, Lanzhou University, Lanzhou 730000, China

[2]Institute of Surface-Earth System Science, Tianjin University, Tianjin 300072, China

Corresponding author: Xin Wang (wxin@lzu.edu.cn)

Abstract. When black carbon (BC) is internally mixed with other atmospheric particles, BC light absorption is effectively enhanced. This study explicitly resolved ~~This study is the first to explicitly resolve~~ the optical properties of coated BC in snow~~the optical properties of coated BC in snow~~, based on core/shell Mie theory and a snow, ice, and aerosol radiative model (SNICAR). Our results indicate that a 'BC coating effect' enhances the reduction of snow albedo by a factor of 1.1–1.8 for a non-absorbing shell and 1.1–1.3 for an absorbing shell, depending on BC concentration, snow grain radius, and core/shell ratio. We develop parameterizations of the BC coating effect for application to climate models, which provides a convenient way to accurately estimate the climate impact of BC in snow. Finally, based on a comprehensive set of in situ measurements across the Northern Hemisphere, we find that the contribution of the BC coating effect to snow light absorption has exceeded that of dust over northern China. Notably, the high enhancements of snow albedo reductions by BC coating effect were found in the Arctic and Tibetan Plateau, suggesting a greater contribution of BC to the retreat of Arctic sea ice and Tibetan glaciers.

1 Introduction

Snow is the most reflective natural substance at Earth's surface and covers more than 30% of global land area (Cohen and Rind, 1991). Snow albedo feedback is considered one of the major energy balance factors of the climate system. Previous observations have revealed that light-absorbing particles (LAPs; e.g., black carbon (BC), organic carbon (OC), and mineral dust) within snow can reduce snow albedo and enhance the absorption of solar radiation (Hadley and Kirchstetter, 2012). As a result, LAPs play a significant role in altering snow morphology and snowmelt processes, and therefore have important effects on local hydrological cycles and global climate (Qian et al., 2009).

Given the importance of the climate feedback caused by LAPs in snow, studies have developed snow radiative models and sought to improve our understanding of the influence of LAP-contaminated snow on climate. For example, Warren and Wiscombe (1980) developed a radiative forcing model based on Mie theory and δ-Eddington approximation, and reported that snow albedo in visible wavelengths could be reduced by 5%–15% when 1000 ng g^{-1} BC is present in snow. Flanner et al. (2007) developed a more comprehensive snow albedo model (the snow, ice, and aerosol radiation model; SNICAR) for multilayer snowpack using the two-stream radiative transfer solution. In addition to BC, the SNICAR model also accounts for the potential effects of dust particles and volcanic ash on snow albedo. Recently, some studies indicated that the mixing state of BC and snow could effectively change snow albedo (Liou et al., 2011, 2014; Flanner et al., 2012; Liu et al., 2012; He et al., 2017, 2018a, b, c~~2011, ~~). ~~Recent~~ Moreover, ~~studies have indicated that~~ snow grain shape also has an important influence on snow albedo (Kokhanovsky and Zege, 2004). Nonspherical snow grains have weaker albedo reduction than snow spheres (He et al., 2018c~~b~~; Dang et al., 2016).~~e.g., Dang et al., 2016).~~

Although efforts have been made to optimize snow albedo models, current models still suffer from major limitations. Studies have indicated that when BC in the atmosphere is coated with other aerosols it can significantly enhance light absorption via a lensing effect compared with uncoated BC, as investigated using model simulations (e.g., Jacobson 2001; Matsui et al., 2018) and experimental measurements (e.g., Cappa et al., 2012; Peng et al., 2016). Moreover, coated BC has been observed to exist for only a few hours after emission in some regions (Moteki et al., 2007; Moffet and Prather, 2009). Global aerosol models that simulate microphysical processes have indicated that most BC is mixed with other particles within 1–5 days (Jacobson, 2001) at all altitudes (Aquila et al., 2011). However, a problem is that whether coated BC is existed in real snowpack because the coating materials (e.g. salts and OC) of coated BC may be dissolved during wet deposition. A recent study observing individual particle structure and mixing states between the glacier–snowpack and atmosphere based on field measurements and laboratory transmission electron microscope (TEM) and energy dispersive X-ray spectrometer (EDX) instrument analysis (Dong et al., 2018) told the truth. They found that the salt-coated BC ~~were~~was still observed in real snowpack in spite of its lower proportion than that in the atmosphere due to the dissolution effect within precipitating snow. For OC, that study didn't observe reduced OC components in LAPs. More notably, that study further found that the proportion of coated BC was even higher in snowpack than that in the atmosphere. All of the above observation results demonstrated that the coated BC particles are existed in real snowpack and even more common than that in the atmosphere. Hence, the climate impacts of BC must be evaluated in the context of the effect of coating on light absorption enhancement.

Although the BC coating effect on light absorption enhancement in the atmosphere is broadly acknowledged, little research has been carried out on snow albedo. Flanner et al. (2007) developed the first radiative transfer model to investigate the coating effect on snow albedo, using sulfate as the BC particle coating with a constant absorption enhancement factor of ~1.5. Subsequently, Wang at al. (2017) used a similar constant light absorption enhancement factor for their spectral albedo model for dirty snow (SAMDS). However, the factor varies with the optical properties of different coatings, the core/shell ratio, wavelength, and other parameters in real environments (Lack and Cappa, 2010; Liu et al., 2017). For example, Liu et al. (2017) reported that the core/shell ratio is a key control on light absorption enhancement. You et al. (2016) suggested that light absorption enhancement is highly correlated with visible or near-infrared (NIR) wavelengths and coating material. Furthermore, a core/shell Mie theory simulation (Lack and Cappa, 2010) found light absorption enhancement was smaller for mildly absorbing coatings (e.g., OC) than non-absorbing coatings (e.g., sulfate). Hence, using a constant enhancement factor will result in biased simulation estimates, against refining our knowledge of the hydrological and climate impacts of BC in snow.

In this study we apply core/shell Mie theory to calculate the optical properties of BC coated with both mildly absorbing OC and non-absorbing sulfate, and use these results within a SNICAR model to evaluate the influence on snow albedo. Parameterizations for the BC coating effect are then developed for application in other snow albedo and climate models. Finally, we estimate the enhancements of snow albedo reductions and associated radiative forcing by the BC coating effect across the Northern Hemisphere, by combining model simulations with in situ observations of BC and OC concentrations in snow.

2 Methods

2.1 Modeling

2.1.1 Optical parameter calculations for coated BC

Figure 1a and 1c shows schematics of light absorption by externally and internally mixed particles (EMP and IMP, respectively). EMP refers to uncoated BC mixed with other particles, while IMP refers to BC that is assumed to be a core coated by another particle acting as a shell (Kahnert et al., 2012). For a non-absorbing shell, overall light absorption includes contributions from the BC core and enhancement absorption from a lensing effect, while for an absorbing shell, the shell itself also contributes to light absorption. The lensing effect means that when BC is coated with the non-absorbing shell (or the absorbing shell), the shell acts as a lens and focuses more photons onto the core than would reach it otherwise, so that the light absorption by the BC core can be enhanced (Bond et al., 2006).

To evaluate the BC coating effect on snow albedo, it is necessary to determine the optical parameters of coated BC. The refractive index (RI) of BC was assumed to be 1.95–0.79i following Lack and Cappa (2010), which is consistent with the original SNICAR model (Flanner et al., 2007). Two types of particle shells (non-absorbing and absorbing) were considered. The non-absorbing shell was represented using sulfate, and its RI was assumed to be $1.55–10^{-6}i$ following the atmospheric study of Bond et al. (2006). The absorbing shell was represented using OC, which is a major light-absorbing particle in snow (Wang et al., 2013). The RI of OC varies with wavelength. Here, a fixed mass absorption coefficient (MAC) for OC of 0.3 m^2 g^{-1} at 550 nm, a real RI of 1.55, and a particle diameter of 200 nm were assumed, Here, a fixed mass absorption coefficient (MAC) for OC of 0.3 m2 g-1 at 550 nm, a real RI of 1.55, and a particle diameter of 200 nm were assumed, following the observations of Yang et al. (2009) and the study of Lack and Cappa (2010)following Lack and Cappa (2010). The uncertainty of snow albedo of coated BC due to OC MAC will be discussed in Section 3.4. Based on Mie theory, an imaginary RI value of $-1.36 \cdot 10^{-2}i$ at 550 nm was calculated. Subsequently, wavelength-dependent imaginary RI values (Figure S1) were derived according to an absorption angstrom exponent (AAE) of −6 (Sun et al., 2007).

For a core/shell-structured particle, the core and shell diameters refer to the BC core diameter and the whole particle diameter, respectively. BC diameters are usually in the range of ~50–120 nm in the atmosphere (Corbin et al., 2018), and are typically larger by ~20 nm in snow due to a removal process via wet deposition (Schwarz et al., 2013). –Therefore, we assumed the BC diameter in snow was 100 nm with a fixed monodisperse size distribution. The uncertainty of snow albedo of coated BC due to BC size distribution will be discussed in Section 3.4~~Therefore, we assumed the BC diameter in snow was 100 nm~~. –The shell diameter was assumed from 110 nm to 300 nm based on Bond et al. (2006). Core and shell diameters, RI, and wavelength were then used in a Mie model to derive optical parameters of the core/shell particle, including single scatter albedo (SSA), asymmetry factor (*g*), and extinction cross-section (Q_{ext}). The mass extinction coefficient (MEC) of the core/shell particle was calculated based on Q_{ext} and the density, given as 1.8 g cm^{-3} for BC (Bond et al., 2006), 1.2 g cm^{-3} for sulfate, and 1.2 g cm^{-3} for OC (Turpin and Lim, 2001).

2.1.2 Snow albedo calculations

We simulated snow albedo with the SNICAR model (Flanner et al., 2007), which calculates the radiative transfer in snowpack based on the theory of Warren and Wiscombe (1980) and a two-stream multilayer radiative approximation (Toon et al., 1989). Here, we summarize only the model features in SNICAR that are crucial to our study. SNICAR allows for a vertical multilayer distribution of snow properties, LAPs, and heating throughout the snowpack column. Input optical parameters (MEC, SSA, and *g*) of snow grains and BC were calculated off-line using Mie theory. SNICAR provides albedo changes from uncoated and sulfate-coated BC on snow, as well as dust particles and volcanic ash (for further details, see Flanner et al., 2007).

In this study, we assumed a homogeneous semi-infinite snowpack and a solar zenith angle of 49.5°, whose cosine value (0.65) represents the insolation-weighted mean solar zenith cosine for sunlit Earth hemisphere (Dang et al., 2015). The snow grain optical effective radius varied from 5100 to 1000 μm (with a 50-μm interval) to characterize snow aging. Meanwhile, BC concentrations were assumed in the range of 0-1000 ng g^{-1} (with a 10-ng g^{-1} interval) to demonstrate clear to polluted snow, which was based on the global field observations with BC concentrations in snowpack mostly below 1000 ng g^{-1} (e.g. Doherty et al., 2010, 2014; Wang et al., 2013; Li et al., 2017, 2018; Pu et al., 2017; Zhang et al., 2017, 2018). These parameters are also applied for parameterizations (see Section 2.3). In addition, we note the SNICAR used in this study was default version that assumes BC-snow external mixing and snow spheres (Flanner et al., 2007). Although the mixing state of BC and snow grains, and snow grain shape can affect the snow albedo, the empirical parameterizations for the effect of BC internally mixed with snow grains on snow albedo has been developed by He et al. (2018cb), and the albedo of a snowpack consisting of nonspherical snow grains can be mimicked by using a smaller grain of spherical shape (Dang et al. 2016). Therefore, users can combine the empirical parameterizations by He et al. (2018cb) and Dang et al. (2016) with the empirical parameterizations by us (see Section 2.3) to study the effect of the internal mixing of BC with snow grains, snow grain shape, and coated BC on snow albedo.

For SNICAR snow albedo simulations of uncoated BC, concentrations of both BC and other particles were input directly. For coated BC, optical parameters (MEC, SSA, and *g*) of IMP (calculated above) were first archived as lookup tables within SNICAR, and then the concentration of IMP was input.

2.2 Calculation of broadband snow albedo

The spectral albedo (α_λ) was integrated over the solar spectrum ($\lambda = 300–2500$ nm) and weighted by the incoming solar irradiance (S_λ) to calculate broadband snow albedo ($\alpha_{integrated}$):

$$\alpha_{integrated} = \frac{\int \alpha_\lambda S_\lambda d_\lambda}{\int S_\lambda d_\lambda} \quad (1)$$

The incoming solar irradiance was a typical surface solar spectrum for mid–high latitudes from January to May, calculated with the Santa Barbara DISORT Atmospheric Radiative Transfer (SBDART) model (Pu et al., 2019), which is one of the most widely used models for radiative transfer simulations (for further details, see Ricchiazzi et al. 1998).

2.3 Parameterizations

In the original SNICAR model, the BC coating effect is simply parameterized with an absorption enhancement of ~1.5 (Flanner et al., 2007). However, the effect of BC coating on snow albedo is widely variable and dependent on BC concentration, core/shell ratio, snow grain size, and the type of particle shell (see Section 3.3). In view of this complexity, more explicit parameterizations were developed in this study:

$$E_{\alpha,\text{integrated}} = \frac{\alpha_{int,\text{integrated}}}{\alpha_{ext,\text{integrated}}} \quad (2)$$

where $\alpha_{ext,\text{integrated}}$ and $\alpha_{int,\text{integrated}}$ are broadband snow albedos for EMP and IMP, respectively. Following a previous empirical formulation (Hadley and Kirchstetter, 2012), $E_{\alpha,\text{integrated}}$ was parameterized as

$$E_{\alpha,\text{integrated,para}} = a_0 \times (C_{BC})^{a_1} + a_2 \quad (3)$$

$$a_1 = b_0 \times (\log_{10}(R_{ef}/50))^{b_1} \quad (4)$$

where $E_{\alpha,\text{integrated,para}}$ is the parameterized $E_{\alpha,\text{integrated}}$, C_{BC} is the BC concentration, and R_{ef} represents the snow grain radius. The terms a_0, a_1, a_2, b_0, and b_1 are the empirical coefficients and dependent on the core/shell ratio and the type of particle shell. To enhance the precision, parameterizations were divided into two groups: the first to account for relatively clean snow (with BC concentrations < 200 ng g^{-1}) and the second for relatively polluted snow (200 ng g^{-1} < BC concentrations < 1000 ng g^{-1}). ~~We note that if BC concentration is larger than 1000 ng g^{-1}, the parameterization for relatively polluted snow is also applicable with a small negative bias based on the results of Section 3.5.~~

2.4 Calculation of in situ snow albedo and radiative forcing

In situ broadband clear-sky ($\alpha_{\text{integrated}}^{\text{clear,in-situ}}$) and cloudy-sky ($\alpha_{\text{integrated}}^{\text{cloudy,in-situ}}$) albedos were calculated separately based on in situ snow-LAP parameters and SBDART simulated clear-sky and cloudy-sky incoming solar irradiance. ~~by~~ We ~~assuming~~

assumed a semi-infinite snowpack due to limited snow depth measurements. BC and OC concentrations were collected from in situ field measurements (e.g. Doherty et al., 2010, 2014; Wang et al., 2013; Li et al., 2017, 2018; Pu et al., 2017; Zhang et al., 2017, 2018). The snow grain radius of 100 (1000) μm was assumed for fresh (old) snow, which is comparable to previous observations ~~of snow grain sizes~~ at mid to high latitudes in winter (Wang et al., 2017; Shi et al., 2020). The value of solar zenith angle was calculated based on the longitude, latitude, and sampling time at each sampling site. The in situ all-sky albedo ($\alpha_{\mathrm{integrated}}^{\mathrm{all-sky,in-situ}}$) was then calculated using weighted clear-sky and cloudy-sky albedos depending on cloud fraction (CF), given as:

$$\alpha_{\mathrm{integrated}}^{\mathrm{all-sky,in-situ}} = \mathrm{CF} \times \alpha_{\mathrm{integrated}}^{\mathrm{cloudy,in-situ}} + (1 - \mathrm{CF}) \times \alpha_{\mathrm{integrated}}^{\mathrm{clear,in-situ}} \quad (5)$$

In situ radiative forcing by LAPs was calculated by multiplying the derived broadband albedo reduction by the downward shortwave flux at the snow surface (Dang et al., 2017). We point out that the radiative forcing was calculated using the January-February average solar radiation for NA and NC, while April-May average solar radiation for the Arctic and TP according to the periods of filed campaigns. In this study, we mainly estimate the relative impact of internal mixing to external mixing on snow albedo and radiative forcing, which is hence not influenced by the chosen solar radiation. ~~We used the downward solar radiation in January (March) and March (May) for fresh snow and old snow at the mid-latitude (Arctic) sampling sites, respectively, consistent with the study of Dang et al. (2017).~~ Figure S2 shows the spatial distributions of solar flux and cloud fraction, which were obtained from the Clouds and the Earth's

Radiant Energy System (CERES) (https://ceres.larc.nasa.gov/products.php?product=SYN1deg).

3 Results and discussion

3.1 Impact on particle light absorption

Figure 1b and 1d shows the light absorption enhancement, E_{abs} for coated BC. E_{abs} is defined as the ratio of the light absorption for ~~an internal mixture~~coated (LA_{int}) versus ~~external mixture~~uncoated BC (LA_{ext}), ~~of BC~~ ($E_{abs} = \frac{LA_{int}}{LA_{ext}}$). ~~Figure 1b and 1d shows light absorption ratios (light absorption enhancement, Eabs) for IMP versus EMP.~~ Based on Bond et al. (2006), we show the most common core/shell ratios (the ratio of the diameter of the whole particle to the BC core) of 1.2, 1.5, 2.0, and 2.5 in real environments to represent the thickness of shells, and we used detailed core/shell ratios from 1.1 to 3.0 (in intervals of 0.1) for parameterizations (see Section 3.5). E_{abs} varies with the wavelength and increases with core/shell ratio, in contrast to the default E_{abs} value used in the original SNICAR model, which remains constant. For a non-absorbing shell, the light absorption of IMP is larger than EMP across all wavelengths (300–1400 nm). For an absorbing shell, E_{abs} is similar to the non-absorbing shell in NIR, but becomes smaller in visible (VIS) light and ultra-violet (UV), which implies the absorbing shell reduces whole-particle light absorption and contributes negatively to E_{abs}. This is because compared with non-absorbing shell, ~~A plausible explanation is that~~ the absorbing shell although ~~shell~~ absorbs additional ~~–~~incident photons, but causes~~ing~~ fewer to reach the core, so that the photons absorbed by the lensing effect and the BC core will be reduced. In such a case, the additional photons absorbed by the shell are fewer than the reduced number of photons absorbed by the lensing effect and the BC core, causing that the total absorption by absorbing shell coated BC will be smaller than non-absorbing shell coated BC (Lack and Cappa, 2010). Furthermore, the absorbing shell reduces E_{abs} to <1 in UV at high core/shell ratios, implying that the lensing effect absorption at those wavelengths cannot recover the BC core absorption reduction, resulting in fewer photons reaching the core, which is similar to the results by Lack and Cappa (2010).

3.2 Impact on spectral snow single-scattering properties and albedos

In real snowpack, BC can effectively enhance snow single-scattering co-albedo (1–ω), but its effect on other snow optical parameters, such as the asymmetry factor and extinction efficiency, is negligible (He et al., 2017). Therefore, we focus our discussion on coating-induced enhancement of snow single-scattering co-albedo ($E_{1-\omega}$), snow albedo (E_{α}), and snow albedo reduction ($E_{\Delta\alpha}$). The $E_{1-\omega}$ is defined as the ratio of snow single-scattering co-albedo with coated BC ($1-\omega_{int}$) versus that with uncoated BC ($1-\omega_{ext}$), ($E_{1-\omega} = \frac{1-\omega_{int}}{1-\omega_{ext}}$). Similar definitions were used for E_{α} ($E_{\alpha} = \frac{\alpha_{int}}{\alpha_{ext}}$) and $E_{\Delta\alpha}$ ($E_{\Delta\alpha} = \frac{\Delta\alpha_{int}}{\Delta\alpha_{ext}}$), where α_{int} and α_{ext} are snow albedos with coated and uncoated BC, and $\Delta\alpha_{int}$ and $\Delta\alpha_{ext}$ are snow albedo reductions due to coated and uncoated BC.

Figure 2 shows the varied 1–ω and $E_{1-\omega}$ depending on different BC concentrations, core/shell ratios, and coating materials. For either non-absorbing shell or absorbing shell, $1-\omega_{int}$ is usually larger than $1-\omega_{ext}$ in VIS~~(Figures 2a versus 2b, 2d versus 2e),~~

~~and~~while t~~T~~he coating effect ~~is distinct in UV and VIS but~~ has little impacts at wavelength > 1200 nm, ~~(Figures 2c and 2f),~~ which is due to that the optical properties of snow is effectively affected by LAPs in ~~UV and~~ VIS, but primarily by snow itself at wavelength > 1200 nm. In addition, $E_{1-\omega}$ increases with increased core/shell ratios, and the wavelength of maximum $E_{1-\omega}$ value is dependent on BC concentrations and core/shell ratios. ~~In addition, when wavelength > ~500 nm, both BC concentration and core/shell ratio have distinct impacts on $E_{1-\omega}$, but when wavelength < ~500 nm, $E_{1-\omega}$ is mainly affected by core/shell ratio.~~ Moreover, absorbing shell shows a negative impact for $E_{1-\omega}$ compared with non-absorbing shell, especially in UV.

Snow albedo is effectively affected by various factors, such as snow grain size, LAP content, solar zenith angle, which has been widely discussed and verified through model simulation and experimental measurements by previous studies (e.g. Warren and Wiscombe, 1980; Hadley and Kirchstetter, 2012; Wang et al., 2017). In this study, we mainly focus on the coating effect of BC on snow albedo. Figure 3 shows the spectral snow albedos for coated (α_{int}) and uncoated BC (α_{ext}), and the ratios (E_{α}) of α_{int} versus α_{ext}. In consistent with 1–ω, the impact of coating effect on snow albedo mainly presents at wavelength < ~1200 nm (Figures 3a versus 3b, 3d versus 3e), where the higher the BC concentration is (or the larger the core/shell ratio is), the larger the difference of snow albedos between ~~snow albedos for~~ uncoated and coated BC is. Hadley and Kirchstetter (2012) also found a smaller snow albedo for internal mixed particles relative to that for external mixed particles. This phenomenon is also obvious on E_α, which decreases with increased BC concentration and core/shell ratios in VIS and NIR (Figure 3c and 3f). For a given BC concentration and core/shell ratio, E_α generally decreases with the wavelength from UV to VIS, then increases from VIS to NIR, which is corresponding to the results of E_{abs} and $E_{1-\omega}$. On the other hand, the E_α for non-absorbing and absorbing shell is comparable with each other at wavelength > ~800 nm. However, when wavelength < ~800 nm, E_α for absorbing shell is larger than that for non-absorbing shell and the difference increases with the decreased wavelength and increased core/shell ratio. Moreover, for absorbing shell, the snow albedo for coated BC is higher than that for uncoated BC at < ~350 nm at large core/shell ratios, which are due to that the light absorption by internal mixed particles for absorbing shell is smaller than that by external mixed particles at those wavelengths as discussed in Section 3.1. These results indicate that the material of particle shell also plays an important role for snow albedo in UV and VIS. We noted that the solar radiative flux is very small at wavelengths < 350 nm, so that the coating effect at those wavelengths may have little contributions to total light absorption and broadband snow albedos, but which may potentially influence the photochemical reactions in snowpack (Grannas et al., 2007).

Furthermore, Figure 4 shows the spectral snow albedo reductions caused by coated ($\Delta\alpha_{int}$) and uncoated BC ($\Delta\alpha_{ext}$), and the ratios ($E_{\Delta\alpha}$) of $\Delta\alpha_{int}$ versus $\Delta\alpha_{ext}$. Generally, $\Delta\alpha_{int}$ is larger than $\Delta\alpha_{ext}$, and core/shell ratio dominates the variations of $E_{\Delta\alpha}$ across the wavelengths of 300-1400 nm, while the impact of BC content mainly focuses on 500-1000 nm. In consistent with $E_{1\text{-}\omega}$ and E_{α}, the impact of the material of particle shell is negligible at wavelength > ~800 nm, but the $E_{\Delta\alpha}$ for absorbing shell is smaller than that for non-absorbing shell at wavelength < ~800 nm. Moreover, the $E_{\Delta\alpha}$ is < 1 for absorbing shell at wavelength < ~350 nm at large core/shell ratios. It is interesting that the coating effect still has an obvious impact on snow albedo reduction at wavelength > ~1200 nm, which is different with $E_{1\text{-}\omega}$ and E_{α}.

has a clear influence on $E_{1-\omega}$ and E_{α} in UV and VIS, but affects $E_{\Delta\alpha}$ across all wavelengths (Figure 2). The core/shell ratio makes a positive contribution to $E_{1-\omega}$ and $E_{\Delta\alpha}$, and a negative contribution to E_{α}. The BC concentration makes a positive contribution to $E_{1-\omega}$ and a negative contribution to $E_{\Delta\alpha}$ and E_{α}. For a given BC concentration and core/shell ratio, $E_{1-\omega}$ and $E_{\Delta\alpha}$ decrease, and E_{α} increases, with longer wavelength from UV to VIS. In addition, the absorbing shell shows a negative influence for $E_{1-\omega}$ and $E_{\Delta\alpha}$, but positive for E_{α} compared with a non-absorbing shell, particularly under UV. Moreover, for an absorbing shell, $E_{1-\omega}$ and $E_{\Delta\alpha}$ are <1, and E_{α} is >1 at approximately <350 nm in the case of high core/shell ratios because of lower light absorption by IMP than EMP at those wavelengths.

3.3 Impact on broadband snow single-scattering properties and albedos

Compared with spectral optical properties, our broadband results have wider implications for the research community. Figure 5 shows the spectrally weighted 1-ω for coated ($1-\omega_{int,\ integrated}$) and uncoated BC ($1-\omega_{ext,\ integrated}$), and the raitos ($E_{1-\omega,\ integrated}$) of $1-\omega_{int,\ integrated}$ versus $1-\omega_{ext,\ integrated}$. In general, $1-\omega_{int,\ integrated}$ is larger than $1-\omega_{ext,}$

integrated, and $E_{1-\omega,\ integrated}$ increased with BC concentration and core/shell ratio, but is little affected by snow grain size. $E_{1-\omega,\ integrated}$ is in a range of 1.0 to ~1.35 and 1.0 to ~1.23 for non-absorbing and absorbing shell, respectively, with BC concentrations within 1000 ng g^{-1} and core/shell ratios of 1.2-2.5. For a given BC concentration and core/shell ratio, $E_{1-\omega,\ integrated}$ for non-absorbing shell is larger than that for absorbing shell. In addition, $E_{1-\omega,\ integrated}$ of the original SNICAR model is closed to that of non-absorbing shell at a core/shell ratio of 1.5.

Figure 6 ~~6a and b~~ shows the spectrally weighted snow albedo for coated ($\alpha_{int,\ integrated}$) and uncoated BC ($\alpha_{ext,\ integrated}$), and the ratios ($E_{\alpha,\ integrated}$) of $\alpha_{int,\ integrated}$ versus $\alpha_{ext,\ integrated}$. ~~$E_{\alpha}$ ($E_{\alpha,\ integrated}$).~~ Generally, $\alpha_{int,\ integrated}$ is smaller than $\alpha_{ext,\ integrated}$ by 0 to ~~XXX~~0.069 (0 to ~~XXX~~0.051), and $E_{\alpha,\ integrated}$ varies~~varied~~ from 1 to ~0.903 (1 to ~0.924) for non-absorbing (absorbing) shell with BC concentrations from 0 to 1000 ng g^{-1}, snow grain radius from 100 μm to 500 μm, and core/shell ratios from 1.2 to 2.5. $E_{\alpha,\ integrated}$ shows a decreased trend with increased BC concentration, core/shell ratio and snow grain size. In addition, the difference between $\alpha_{ext,\ integrated}$ and $\alpha_{int,\ integrated}$ (or $E_{\alpha,\ integrated}$) ~~$E_{\alpha,\ integrated}$~~ for non-absorbing shell is larger (or smaller) than that for absorbing shell. If considering these coating effects in real environments. For example, in clean snow, such as North American with a typical BC concentration of ~50 ng g^{-1} (Doherty et al., 2014), the difference between $\alpha_{ext,\ integrated}$ and $\alpha_{int,\ integrated}$~~$E_{\alpha,\ integrated}$~~ is in a range of ~~XXX~~0.002-~~XXX~~0.017 ~~0.979-0.998~~ and ~~XXX~~0.001-~~XXX~~0.012 ~~0.985-0.998~~ for non-absorbing and absorbing shell, respectively, with core/shell ratios of 1.2-2.5 and snow grain radius of 100-500 μm. In contrast, in polluted snow, such as Northeastern China, BC concentration is typically ~1000 ng g^{-1} in industrial regions. the difference between $\alpha_{ext,\ integrated}$ and $\alpha_{int,\ integrated}$ $E_{\alpha,\ integrated}$ ranges from XXX0.008-XXX0.069 and XXX0.007-XXX0.051 0.903 to 0.991 and 0.924 to 0.992 for non-absorbing and absorbing shell, respectively, lower than the results in clean snow. The results show that the impact of coating effect on snow albedo can leads the snow albedo reduced by ~2% in clean snow and ~10% in polluted snow for internal mixed particles relativecoated BC tothan that for external mixed particlesuncoated BC. In addition, the sensitivity of $E_{\alpha,\ integrated}$ to BC decreases with increasing BC concentration due to the nonlinear effect of BC on snow albedo (Flanner et al., 2007).. For example, the difference of $E_{\alpha,\ integrated}$ is 0.009 (0.006) between BC concentrations of 100 and 200 ng g^{-1}, but only 0.003 (0.002) between BC concentrations of 900 and 1000 ng g^{-1} at a core/shell ratio of 2.5 and snow grain radius of 200 μm for non-absorbing shell (absorbing shell). We note again that the original SNICAR model only reflects the impact of coating effect on snow albedo at an intermediate core/shell ratio of ~1.5.

Figure 7 shows the spectrally weighted snow albedo reductions by coated ($\Delta\alpha_{int,\ integrated}$) and uncoated BC ($\Delta\alpha_{ext,\ integrated}$), and the ratios ($E_{\Delta\alpha,\ integrated}$) of $\Delta\alpha_{int,\ integrated}$ versus $\Delta\alpha_{ext,\ integrated}$. Different from $E_{\alpha,\ integrated}$, $E_{\Delta\alpha,\ integrated}$ is dominated by core/shell ratio, but little dependent on snow grain size (Figures 7c and 6f). In addition, $E_{\Delta\alpha,\ integrated}$ presents a slight decreased trend with increased BC concentration. Comparing Figure

7c and f, we find that the material of particle shell presents a distinct impact on $E_{\Delta\alpha, integrated}$. $E_{\Delta\alpha, integrated}$ mostly falls in a range of 1.11 to ~1.80 (1.10 to ~1.33) for non-absorbing (absorbing) shell with core/shell ratios from 1.2 to 2.5. Our results were comparable with the previous study that the snow albedo reduction of BC-snow internal mixing is larger than external mixing by a factor of 0.2-1.0 (He et al., 2018cb). On the other hand, the $E_{\Delta\alpha, integrated}$ from the original SNICAR model only shows a small variation of 1.23–1.31. This is similar to a non-absorbing shell with a core/shell ratio of ~1.5, which implies the original SNICAR model only reflects a coating effect on snow albedo reduction at an intermediate core/shell ratio and may lead to possible biases of -10% to 50% in snow albedo reduction calculation.

Core/shell ratios dominate variations in spectrally weighted $E_{1-\omega, integrated}$, $E_{\alpha, integrated}$, and $E_{\Delta\alpha, integrated}$ (Figure 3). Snow grain size and BC concentration show a negative contribution to $E_{\alpha, integrated}$, but barely affect $E_{\Delta\alpha, integrated}$. However, the type of particle shell has a significant impact on $E_{1-\omega, integrated}$, $E_{\alpha, integrated}$, and $E_{\Delta\alpha, integrated}$. Compared with $E_{1-\omega, integrated}$ and $E_{\alpha, integrated}$, $E_{\Delta\alpha, integrated}$ has a more direct influence on radiative forcing and climate change. $E_{\Delta\alpha, integrated}$ largely falls within a range of 1.11 to ~1.80 for a non-absorbing shell, which exceeds the values for an absorbing shell (1.10 to ~1.33) by a factor of 1.0–1.35 (with BC concentrations within 1000 ng g^{-1}, a snow grain radius of 100–500 μm, and core/shell ratios from 1.2 to 2.5). Our results were comparable with the previous study that the snow albedo reduction of BC-snow internal mixing is larger than external mixing by a factor of 0.2-1.0 (He et al., 2018b). In contrastOn the other hand, the $E_{\Delta\alpha,\ integrated}$ from the original SNICAR model only shows a small variation of 1.23–1.31. This is similar to a non-absorbing shell with a core/shell ratio of ~1.5, which implies the original SNICAR model only reflects a coating effect on snow albedo reduction at an intermediate core/shell ratio and may lead to possible biases of -10% to 50% in snow albedo reduction calculation.

3.4 Uncertainties

Although the imaginary RI value of OC has been theoretically calculated (Section 2.1), we note that in real snowpack there is large uncertainty because the types and optical properties of OC varies spatially and temporally due to different emission sources and photochemical reactions in the atmosphere (e.g. Lack and Cappa, 2010). To address this issue, we tested the degree of influence of imaginary RI on $E_{\alpha,\ integrated}$, and $E_{\Delta\alpha,\ integrated}$ values by increasing and decreasing the calculated imaginary RI by 50% (Figure S1), which studies have shown to be plausible (e.g., Lack et al., 2012). We find imaginary RI uncertainty to be ±1% for $E_{\alpha,\ integrated}$ and ±5% for $E_{\Delta\alpha,\ integrated}$.

In addition, observations show large variation in the size distribution of atmospheric and snow BC particles (Schwarz et al., 2013), which can affect snow optical properties and albedo (He at al., 2018). Therefore, we examined the effects of BC particle size on $E_{\alpha,\ integrated}$ and $E_{\Delta\alpha,\ integrated}$ with two additional BC diameters of 50 nm and 150 nm, which are within observed size ranges (Schwarz et al., 2013) and are comparable to BC particle sizes used in other studies (e.g. He et al., 2018b). We find the uncertainty attributed to BC diameter is ±1% for $E_{\alpha,\ integrated}$ and ±13% for $E_{\Delta\alpha,}$

integrated. According to Equation 2, the uncertainty for $E_{\alpha,\ integrated}$ is equivalent to that for snow albedo and the uncertainty for $E_{\Delta\alpha,\ integrated}$ is equivalent to that for snow albedo reduction. ThereforeOverall, the total uncertainty related to imaginary RI and BC diameter is ±1.4% for $E_{\alpha,\ integrated}$ (snow albedo) and ±13.9% for $E_{\Delta\alpha,\ integrated}$ (snow albedo reduction).

Another important issue is that in real environments, BC mixtures with other species are likely much more complex than uniform coatings on spheres, hence a core-shell assumption seems somewhat dubious. .However, a recent study observing individual particle structure and mixing states between the glacier–snowpack and atmosphere (Dong et al., 2018) found that fresh BC particles are generally characterized with fractal morphology, which has a large quantity in the atmosphere. In contrast, in the snowpack, aged BC particles dominated the BC content and the mixing states of aged BC particles change largely to the internal mixing forms with BC as the core. This process is characterized by the initial transformation from a fractal structure to spherical morphology and the subsequent growth of fully compact particles during the transport and deposition process. Therefore, a core-shell assumption for coated BC in snowpack seems to be plausible. In addition, most filed measurements can not capture the explicit structure of coated BC due to limited observation methods (e.g. Doherty et al., 2010, 2014; Wang et al., 2013; Li et al., 2017, 2018; Pu et al., 2017; Zhang et al., 2017, 2018), therefore even if a model for explicit BC structure was developed, researchers are hard to use it for studying the effect of coated BC on snow albedo reductions at present.

Moreover, a core-shell assumption for coated BC in the atmosphere has been widely applied by most global climate models (e.g. Jacobson, 2001; Bond et al. 2013), so that our parameterizations for coated BC in snowpack can be easily linked to them. In summary, we indicate that a core-shell assumption for coated BC in snowpack is plausible and practical for field observations and model simulations at present in despite of the possible uncertainties. However, with the developments of measurement methods and climate models, building a more explicit structure for coated BC in snowpack is actually needed in the future.

3.5 Parameterizations of the coating effect

Figure 874 compares parameterized $E_{\alpha,\ integrated,\ para}$ with SNICAR-modeled $E_{\alpha,\ integrated}$, and Tables S1 and S2 list the empirical coefficients (see Section 2.3) derived from nonlinear regression processes. This parameterization is under the assumptions of semi-infinite snowpack, BC-snow external mixing, and spherical snow grains as mentioned in Section 2. Generally, $E_{\alpha,\ integrated,\ para}$ and $E_{\alpha,\ integrated}$ show a strong correlation, with $R^2 = 0.988$ (0.986) for a non-absorbing shell and $R^2 = 0.987$ (0.986) for an absorbing shell in relatively clean (polluted) snow, and root mean squared errors of $1.81 \cdot 10^{-3}$ ($4.70 \cdot 10^{-3}$) and $1.41 \cdot 10^{-3}$ ($3.76 \cdot 10^{-3}$), respectively. Biases for $E_{\alpha,\ integrated,\ para}$ are smallest for intermediate BC concentrations and snow grain radius, but become relatively larger at extremely low or high values, due mainly to processes within the nonlinear regression method. In addition, the snow grain size has small impacts on the accuracy of parameterized results, so that the parameterizations can be applied in either fresh snow or old snow types. Overall, the $E_{\alpha, integrated}$ can be well reproduced by $E_{\alpha, integrated, para}$ and the parameterizations are applicable in various snow pollution conditions with BC concentrations from 0-1000 ng g^{-1}, core/shell ratios from 1.1 to 3.0, and different coating materials (non-absorbing and absorbing shell). We note that if BC concentration is larger than 1000 ng g^{-1}, the parameterization for relatively polluted snow is also applicable with a small negative (positive) bias.Overall, the $E_{\alpha, integrated}$ can be well reproduced by $E_{\alpha, integrated, para}$ for both a non-absorbing and absorbing shell under the conditions of both relatively clean and polluted snow.

Therefore, other studies can estimate the coating effect of BC on snow albedos and radiative forcing very conveniently by combining the original SNICAR or other snow radiative forcing model with our new parameterizations, which can may reduce snow albedo simulation bias. For example, Wang et al. (2017) compared observations and model simulations of snow albedo reduction in northern China. They found simulated results overestimated snow albedo by ~0.06 in polluted snow, despite considering the effects of all LAP types (BC, OC, and dust), snow grain type, and snow depth. However, if the coating effect is taken into account and the new parameterizations are applied (according to their measured LAPs and snow parameters), the difference between simulation and observation is reduced to ~0.02, thereby improving the simulation. FurthermoreOn the other hand, although most global climate models (GCMs) account for coated BC in the atmosphere, , although most global climate models (GCMs) account for internal mixing of atmospheric BC, they barely consider the coating effect for BC in snow (Bond et al., 2013). In addition, different GCMs apply different types of snow radiative transfer models, which means that one physical mechanism responsible for the BC coating effect in snow cannot be suitable for all GCMs. Hence, our parameterizations ~~is~~are good for the climate models to have an option for BC coating effects in snow~~In this case our parameterizations are particularly helpful, as they are easily used in any GCM and improve understanding of how BC in snow influences local hydrological cycles and global climate~~.

3.6 Measurement-based estimate of coating effect

To evaluate the coating effect of BC on both snow albedo and radiative forcing in real snowpack, we collected in situ measurements of BC and OC concentrations in snow (Figure 89~~5~~) during field campaigns in the Arctic in spring 2007–2009 (Doherty et al., 2010), North America in January–March 2013 (Doherty et al., 2014), northern China in January–February 2010 and 2012 (Ye et al., 2012; Wang et al., 2013), and the Tibetan Plateau in spring 2010 and 2012 (Wang et al., 2013; Li et al., 2017, 2018; Pu et al., 2017; Zhang et al., 2017, 2018). Measurements are separated into four geographical regions (Figure 89~~5~~c): the Arctic, North America (NA), northern China (NC), and the Tibetan Plateau (TP). An absorbing shell of OC was assumed in measured snowpack, which is plausible because previous studies have found that OC is the dominant coating in the atmosphere (e.g., Cappa et al., 2012) and snow (Dong et al., 2018). The OC/BC mass ratio is generally from 1 to 10, with the corresponding core/shell ratio from 1.3 to 2.5 (Figure 89~~5~~b). The average core/shell ratio was highest

(2.45) in the TP, followed by 1.92 and 1.81 in the Arctic and NC, respectively, and lowest (1.31) in NA (Figure 895d). These results reveal the BC coating effect had a larger impact on snow albedo in the TP than in other regions. In this study, the assumption that all measured OC resides as coating on BC particles were mainly used to show the upper bound of coating effect on snow albedo reduction, which wasis comparable with the previous studies (e.g. He et al. 2018c).

Figure 910 shows the statistics for snow albedo reductions and radiative forcing in different regions for fresh snow (snow grain radius =100 μm) and old snow (snow grain radius =1000 μm). The spatial distributions of snow albedo reductions and radiative forcing are presented in Figure S3 and S4. Briefly, the TP snowpack suffers the highest snow albedo reduction (0.066), and the regional average snow albedo reductions are lower in NC (0.055), NA (0.009), and the Arctic (0.007) for fresh snow in the case of external mixing (Figure 10a). Accordingly, the regional average radiative forcing is 11.63, 4.42, 0.97, and 0.56 W m^{-2} in TP, NC, NA, and the Arctic (Figure 910b). In the case of internal mixing, the regional average snow albedo reductions are 0.084, 0.065, 0.011, and 0.009 in TP, NC, NA, and the Arctic, with the corresponding radiative forcing of 14.84, 5.51, 1.11, and 0.69 W m^{-2}. Figure 101 shows the comparisons of internal mixing to external mixing. Figure 6 presents the coating effect on snow albedo reduction and radiative forcing based on measured BC in real snowpack, and Figures S3–S5 show spatial distributions and statistics. For fresh snow, we find that IMP coated BC results in greater snow albedo reductions compared with EMP uncoated

BC by factors of 1.27, 1.19, 1.13, and 1.23 in the TP, NC, NA, and the Arctic, respectively (Figures 1~~0~~1~~6~~a and 1~~0~~1b). Correspondingly, we find that ~~IMP~~ the coating effect leads radiative forcing by 1.27, 1.20, 1.14, and 1.22 for these same regions. The highest (lowest) enhancement was found in the TP (NA), which corresponds to the highest (lowest) OC/BC mass ratio and core/shell ratio in the TP (NA). For old snow~~,~~ , the regional average snow albedo reductions are 0.17 (0.21), 0.14 (0.17), 0.028 (0.033) and 0.022 (0.027) in TP, NC, NA, and the Arctic for external (internal) mixing (Figure ~~9~~10c). The corresponding radiative forcing are 38.2 (47.6), 19.2 (22.7), 4.6 (5.2) and 3.6 (4.6) W m^{-2} (Figure ~~9~~10d). T~~t~~he enhancement of snow albedo reductions due to the BC coating effect are 1.24, 1.15, 1.13, and 1.23 in TP, NC, NA, and the Arctic, respectively (Figure 1~~0~~1c). The corresponding radiative forcing reductions are 1.24, 1.16, 1.14, and 1.22 (Figure 1~~0~~1d). The enhancement shows a slight decrease with snowpack aging, which is consistent with the results in Figure 7~~3~~. Of note, we found the contribution of coating effect to light absorption has exceeded dust over most areas of northern China after comparing with previous studies of dust in snow (Wang et al., 2013, 2017; Pu et al., 2017), which further demonstrated the critical role of BC coatings in snow albedo evaluation.

In contrast to previous studies, we note that enhanced light absorption in snow from the BC coating effect should be taken into account, especially in the Arctic and the TP. Arctic sea ice has shown a sharp decline in recent decades (Ding et al., 2019), and climate models predict a continued decreasing trend (Liu et al., 2020) that is likely to perturb the Earth system and influence human activities (Meier et al., 2014). Multi-model ensemble simulations indicate that greenhouse gases cannot fully explain this decline, and recent studies have proposed that BC deposition in snow and sea ice is an important additional contributor (e.g., Ramanathan and Carmichael, 2008). Furthermore, the TP holds the largest ice mass outside polar regions, and acts as a water 'storage tower' for more than 1 billion people in South and East Asia. Tibetan glaciers have rapidly retreated over the last 30 years (Yao et al., 2012), raising the possibility that many glaciers and their fresh water supplies could disappear by the middle of the 21st century. Observed evidence suggests that BC deposition is a significant contributing factor to this retreat (Xu et al., 2009), but quantitatively modeling the effect of BC on glacier dynamics is a challenge, partly because of incomplete radiative transfer mechanisms within models. Due to the significant contribution of BC to retreating Arctic sea ice and Tibetan glaciers, and the strong enhancement of light absorption by coated BC, the coating effect must now be considered in climate models that are designed to accurately reconstruct both the historical record and future change.

4 Conclusions

This study evaluated the effect of BC coating on snow albedo and radiative forcing by combing core/shell Mie theory and the snow-albedo model SNICAR. We found that the coating effect ~~reduces~~ enhances snow albedo reduction by a factor of 1.11–1.80 for a non-absorbing shell and 1.10–1.33 for an absorbing shell, when BC concentrations are within 1000 ng g^{-1}, the snow grain radius is 100–500 μm, and the core/shell ratio is

1.2–2.5. The core/shell ratio plays a dominant role in reducing snow albedo. Furthermore, an absorbing shell causes a smaller snow albedo reduction than a non-absorbing shell because of a lensing effect, whereby the absorbing shell reduces photon absorbance in the BC core. Our results can effectively account for the complex enhancement of snow albedo reduction due to coating effect in real environments.

Parameterizations for the coating effect are further developed for use in snow albedo and climate models. Parameterized and simulated results show strong correlations for both clean and polluted snowpack. The root mean squared error of parameterized $E_{\alpha,\ \mathrm{integrated,\ para}}$ is low ($1.41 \cdot 10^{-3}$). A list of empirical coefficients for parameterizations is provided for most seasonal snowpack field cases, with BC concentrations within 1000 ng g^{-1}, snow grain sizes from 5100–1000 μm, and core/shell ratios from 1.1 to 3.0. We demonstrate that parameterizations can reduce simulation bias for local experiments in snow albedo models and, more importantly, can be applied to GCMs to improve our understanding of how BC in snow affects local hydrological cycles and global climate.

Based on a comprehensive set of field measurements across the Northern Hemisphere, the BC coating effect in real snowpack was evaluated by assuming the presence of an absorbing OC shell. The enhancement of snow albedo reduction was 1.133–1.273 and enhancement of radiative forcing was 1.1435–1.274, which exceeds the contribution of dust to snow light absorption over most areas of northern China. Of note, the greatest enhancements were detected on the Tibetan Plateau and in the Arctic, which will likely contribute to further Arctic sea ice and Tibetan glacier retreat. Our findings indicate that the coating effect must be considered in future climate models, in particular to more accurately evaluate the climate of the Tibetan Plateau and the Arctic.

Conflict of interest

The authors declare that they have no conflict of interest.

Acknowledgments

This research was supported jointly by the National Science Fund for Distinguished Young Scholars (42025102), the National Key R&D Program of China (2019YFA0606801), , the National Natural Science Foundation of China (42075061, 41975157 and 41775144), and the China Postdoctoral Science Foundation (2020M673530).

Author contributions

X Wang and W Pu invited the project. W Pu and X Wang designed the study. W Pu wrote the paper with contributions from all co-authors. TL Shi processed and analyzed the data.

References

Aquila, V., Hendricks, J., Lauer, A., Riemer, N., Vogel, H., Baumgardner, D., Minikin, A., Petzold, A., Schwarz, J., and Spackman, J.: MADE-in: A new aerosol microphysics submodel for global simulation of insoluble particles and their mixing state, Geosci. Model Dev., 4, 325-355, 2011.

Bond, T. C., Habib, G., and Bergstrom, R. W.: Limitations in the enhancement of visible light absorption due to mixing state, J. Geophys. Res.-Atmos., 111, D20, 2006.

Bond, T. C., Doherty, S. J., Fahey, D. W., Forster, P. M., Berntsen, T., DeAngelo, B. J., Flanner, M. G., Ghan, S., Karcher, B., Koch, D., Kinne, S., Kondo, Y., Quinn, P. K., Sarofim, M. C., Schultz, M. G., Schulz, M., Venkataraman, C., Zhang, H., Zhang, S., Bellouin, N., Guttikunda, S. K., Hopke, P. K., Jacobson, M. Z., Kaiser, J. W., Klimont, Z., Lohmann, U., Schwarz, J. P., Shindell, D., Storelvmo, T., Warren, S. G., and Zender, C. S.: Bounding the role of black carbon in the climate system: A scientific assessment, J. Geophys. Res.-Atmos., 118, 5380-5552, 2013.

Cappa, C. D., Onasch, T. B., Massoli, P., Worsnop, D. R., Bates, T. S., Cross, E. S., Davidovits, P., Hakala, J., Hayden, K. L., Jobson, B. T., Kolesar, K. R., Lack, D. A., Lerner, B. M., Li, S. M., Mellon, D., Nuaaman, I., Olfert, J. S., Petaja, T., Quinn, P. K., Song, C., Subramanian, R., Williams, E. J., and Zaveri, R. A.: Radiative Absorption Enhancements Due to the Mixing State of Atmospheric Black Carbon, Science, 337, 1078-1081, 2012.

Cohen, J., and Rind, D.: The effect of snow cover on the climate, J. Climate, 4, 689-706, 1991.

Corbin, J. C., Pieber, S. M., Czech, H., Zanatta, M., Jakobi, G., Massabò, D., Orasche, J., El Haddad, I., Mensah, A. A., and Stengel, B.: Brown and black carbon emitted by a marine engine operated on heavy fuel oil and distillate fuels: optical properties, size distributions, and emission factors, J. Geophys. Res.-Atmos., 123, 6175-6195, 2018.

Dang, C., Brandt, R. E., and Warren, S. G.: Parameterizations for narrowband and broadband albedo of pure snow and snow containing mineral dust and black carbon, J Geophys Res-Atmos, 120, 5446-5468, 2015.

Dang, C., Fu, Q., and Warren, S. G.: Effect of Snow Grain Shape on Snow Albedo, J. Atmos. Sci., 73, 3573-3583, 2016.

Dang, C., Warren, S. G., Fu, Q., Doherty, S. J., and Sturm, M.: Measurements of light-absorbing particles in snow across the Arctic, North America, and China: effects on surface albedo, J. Geophys. Res.-Atmos., 122, 10149-10168, 2017.

Ding, Q., Schweiger, A., L'Heureux, M., Steig, E. J., Battisti, D. S., Johnson, N. C., Blanchard-Wrigglesworth, E., Po-Chedley, S., Zhang, Q., and Harnos, K.: Fingerprints of internal drivers of Arctic sea ice loss in observations and model simulations, Nat. Geosci., 12, 28-33, 2019.

Doherty, S. J., Warren, S. G., Grenfell, T. C., Clarke, A. D., and Brandt, R. E.: Light-absorbing impurities in Arctic snow, Atmos. Chem. Phys., 10, 11647-11680, 2010.

Doherty, S. J., Dang, C., Hegg, D. A., Zhang, R., and Warren, S. G.: Black carbon and other light-absorbing particles in snow of central North America, J. Geophys. Res.-Atmos., 119, 12807-12831, 2014.

Dong, Z., Kang, S., Qin, D., Shao, Y., Ulbrich, S., and Qin, X.: Variability in individual particle structure and mixing states between the glacier–snowpack and atmosphere in the northeastern Tibetan Plateau, The Cryosphere, 12, 3877-3890, 2018.

Flanner, M. G., Liu, X., Zhou, C., Penner, J. E., and Jiao, C.: Enhanced solar energy absorption by internally-mixed black carbon in snow grains, Atmos Chem Phys, 12, 4699-4721, 2012.

Flanner, M. G., Zender, C. S., Randerson, J. T., and Rasch, P. J.: Present-day climate forcing and response from black carbon in snow, J. Geophys. Res., 112, D11, 2007.

Grannas, A. M., Jones, A. E., Dibb, J., Ammann, M., Anastasio, C., Beine, H. J., Bergin, M., Bottenheim, J., Boxe, C. S., Carver, G., Chen, G., Crawford, J. H., Domine, F., Frey, M. M., Guzman, M. I., Heard, D. E., Helmig, D., Hoffmann, M. R., Honrath, R. E., Huey, L. G., Hutterli, M., Jacobi, H. W., Klan, P., Lefer, B., McConnell, J., Plane, J., Sander, R., Savarino, J., Shepson, P. B., Simpson, W. R., Sodeau, J. R., von Glasow, R., Weller, R., Wolff, E. W., and Zhu, T.: An overview of snow photochemistry: evidence, mechanisms and impacts, Atmos Chem Phys, 7, 4329-4373, 2007.

Hadley, O. L., and Kirchstetter, T. W.: Black-carbon reduction of snow albedo, Nat. Clim. Change, 2, 437-440, 2012.

He, C. L., Takano, Y., Liou, K. N., Yang, P., Li, Q., Chen, F., He, C., Takano, Y., Liou, K. N., and Yang, P.: Impact of Snow Grain Shape and Black Carbon-Snow Internal Mixing on Snow Optical Properties: Parameterizations for Climate Models, J. Climate, 30, 10019-10036, 2017.

~~He, C. L., Liou, K. N., and Takano, Y.: Resolving Size Distribution of Black Carbon Internally Mixed With Snow: Impact on Snow Optical Properties and Albedo, Geophys. Res. Lett., 45, 2697-2705, 2018.~~He, C. L., Flanner, M. G., Chen, F., Barlage, M., Liou, K. N., Kang, S. C., Ming, J., and Qian, Y.: Black carbon-induced snow albedo reduction over the Tibetan Plateau: uncertainties from snow grain shape and aerosol-snow mixing state based on an updated SNICAR model, Atmos Chem Phys, 18, 11507-11527, 2018a.

He, C. L., Liou, K. N., and Takano, Y.: Resolving Size Distribution of Black Carbon Internally Mixed With Snow: Impact on Snow Optical Properties and Albedo, Geophys. Res. Lett., 45, 2697-2705, 2018b.

He, C. L., Liou, K. N., Takano, Y., Yang, P., Qi, L., and Chen, F.: Impact of Grain Shape and Multiple Black Carbon Internal Mixing on Snow Albedo: Parameterization and Radiative Effect Analysis, J Geophys Res-Atmos, 123, 1253-1268, 2018c.

Jacobson, M. Z.: Strong radiative heating due to the mixing state of black carbon in

atmospheric aerosols, Nature, 409, 695-697, 2001.
Kahnert, M., Nousiainen, T., Lindqvist, H., and Ebert, M.: Optical properties of light absorbing carbon aggregates mixed with sulfate: assessment of different model geometries for climate forcing calculations, Opt. Express, 20, 10042-10058, 2012.
Kokhanovsky, A. A., and Zege, E. P.: Scattering optics of snow, Appl Optics, 43, 1589-1602, 2004.
Lack, D. A., and Cappa, C. D.: Impact of brown and clear carbon on light absorption enhancement, single scatter albedo and absorption wavelength dependence of black carbon, Atmos. Chem. Phys., 10, 4207-4220, 2010.
Lack, D. A., Langridge, J. M., Bahreini, R., Cappa, C. D., Middlebrook, A. M., and Schwarz, J. P.: Brown carbon and internal mixing in biomass burning particles, PNAS, 109, 14802-14807, 2012.
Li, X., Kang, S., He, X., Qu, B., Tripathee, L., Jing, Z., Paudyal, R., Li, Y., Zhang, Y., and Yan, F.: Light-absorbing impurities accelerate glacier melt in the Central Tibetan Plateau, Sci. Total Environ., 587, 482-490, 2017.
Li, X., Kang, S., Zhang, G., Qu, B., Tripathee, L., Paudyal, R., Jing, Z., Zhang, Y., Yan, F., and Li, G.: Light-absorbing impurities in a southern Tibetan Plateau glacier: Variations and potential impact on snow albedo and radiative forcing, Atmos. Res., 200, 77-87, 2018.
Liu, D. T., Whitehead, J., Alfarra, M. R., Reyes-Villegas, E., Spracklen, D. V., Reddington, C. L., Kong, S. F., Williams, P. I., Ting, Y. C., Haslett, S., Taylor, J. W., Flynn, M. J., Morgan, W. T., McFiggans, G., Coe, H., and Allan, J. D.: Black-carbon absorption enhancement in the atmosphere determined by particle mixing state, Nat. Geosci., 10, 184-U132, 2017.
Liu, J., Wu, D., Liu, G., Mao, R., Chen, S., Ji, M., Fu, P., Sun, Y., Pan, X., and Jin, H.: Impact of Arctic amplification on declining spring dust events in East Asia, Clim. Dyn., 54, 1913-1935, 2020.

Liou, K. N., Takano, Y., and Yang, P.: Light absorption and scattering by aggregates: Application to black carbon and snow grains, J Quant Spectrosc Ra, 112, 1581-1594, 2011.
Liou, K. N., Takano, Y., He, C., Yang, P., Leung, L. R., Gu, Y., and Lee, W. L.: Stochastic parameterization for light absorption by internally mixed BC/dust in snow grains for application to climate models, J Geophys Res-Atmos, 119, 7616-7632, 2014.
Liu, X., Zhou, C., Penner, J. E., and Jiao, C.: Enhanced solar energy absorption by internally-mixed black carbon in snow grains, Atmos. Chem. Phys., 12, 4699–4721, https://doi.org/10.5194/acp-12-4699-2012, 2012.
Matsui, H., Hamilton, D. S., and Mahowald, N. M.: Black carbon radiative effects highly sensitive to emitted particle size when resolving mixing-state diversity, Nat. Commun., 9, 1-11, 2018.
Meier, W. N., Hovelsrud, G. K., Van Oort, B. E., Key, J. R., Kovacs, K. M., Michel,

C., Haas, C., Granskog, M. A., Gerland, S., and Perovich, D. K.: Arctic sea ice in transformation: A review of recent observed changes and impacts on biology and human activity, Rev. Geophys., 52, 185-217, 2014.

Moffet, R. C., and Prather, K. A.: In-situ measurements of the mixing state and optical properties of soot with implications for radiative forcing estimates, PNAS, 106, 11872-11877, 2009.

Moteki, N., Kondo, Y., Miyazaki, Y., Takegawa, N., Komazaki, Y., Kurata, G., Shirai, T., Blake, D. R., Miyakawa, T., and Koike, M.: Evolution of mixing state of black carbon particles: Aircraftmeasurements over the western Pacific in March 2004, Geophys. Res. Lett., 34, L11803, 2007.

Peng, J. F., Hu, M., Guo, S., Du, Z. F., Zheng, J., Shang, D. J., Zamora, M. L., Zeng, L. M., Shao, M., Wu, Y. S., Zheng, J., Wang, Y., Glen, C. R., Collins, D. R., Molina, M. J., and Zhang, R. Y.: Markedly enhanced absorption and direct radiative forcing of black carbon under polluted urban environments, PNAS, 113, 4266-4271, 2016.

Pu, W., Wang, X., Wei, H., Zhou, Y., Shi, J., Hu, Z., Jin, H., and Chen, Q.: Properties of black carbon and other insoluble light-absorbing particles in seasonal snow of northwestern China, The Cryosphere, 11, 1213-1233, 2017.

Pu, W., Cui, J. C., Shi, T. L., Zhang, X. L., He, C. L., and Wang, X.: The remote sensing of radiative forcing by light-absorbing particles (LAPs) in seasonal snow over northeastern China, Atmos. Chem. Phys., 19, 9949-9968, 2019.

Qian, Y., Gustafson, W. I., Leung, L. R., and Ghan, S. J.: Effects of soot-induced snow albedo change on snowpack and hydrological cycle in western United States based on Weather Research and Forecasting chemistry and regional climate simulations, J. Geophys. Res.-Atmos., 114, D3, 2009.

Ramanathan, V., and Carmichael, G.: Global and regional climate changes due to black carbon, Nat. Geosci., 1, 221-227, 2008.

Ricchiazzi, P., Yang, S., Gautier, C., and Sowle, D.: SBDART: A research and teaching software tool for plane-parallel radiative transfer in the Earth's atmosphere, Bull. Amer. Meteor. Soc., 79, 2101-2114, 1998.

Schwarz, J. P., Gao, R. S., Perring, A. E., Spackman, J. R., and Fahey, D. W.: Black carbon aerosol size in snow, Sci. Rep., 3, 1356, 2013.

Shi, T., Pu, W., Zhou, Y., Cui, J., Zhang, D., and Wang, X.: Albedo of Black Carbon-Contaminated Snow Across Northwestern China and the Validation With Model Simulation, J. Geophys. Res.-Atmos., 125, e2019JD032065, 2020.

Sun, H. L., Biedermann, L., and Bond, T. C.: Color of brown carbon: A model for ultraviolet and visible light absorption by organic carbon aerosol, Geophys. Res. Lett., 34, L17813, 2007.

Toon, O. B., Mckay, C. P., Ackerman, T. P., and Santhanam, K.: Rapid Calculation of Radiative Heating Rates and Photodissociation Rates in Inhomogeneous Multiple-Scattering Atmospheres, J. Geophys. Res.-Atmos., 94, 16287-16301, 1989.

Turpin, B. J., and Lim, H. J.: Species contributions to PM2.5 mass concentrations:

Revisiting common assumptions for estimating organic mass, Aerosol Sci. Tech., 35, 602-610, 2001.
Wang, X., Doherty, S. J., and Huang, J.: Black carbon and other light-absorbing impurities in snow across Northern China, J. Geophys. Res.-Atmos., 118, 1471-1492, 2013.
Wang, X., Pu, W., Ren, Y., Zhang, X. L., Zhang, X. Y., Shi, J. S., Jin, H. C., Dai, M. K., and Chen, Q. L.: Observations and model simulations of snow albedo reduction in seasonal snow due to insoluble light-absorbing particles during 2014 Chinese survey, Atmos. Chem. Phys., 17, 2279-2296, 2017.
Warren, S. G., and Wiscombe, W. J.: A Model for the Spectral Albedo of Snow. 2: Snow Containing Atmospheric Aerosols, J. Atmos. Sci., 37, 2734-2745, 1980.
Xu, B. Q., Cao, J. J., Hansen, J., Yao, T. D., Joswia, D. R., Wang, N. L., Wu, G. J., Wang, M., Zhao, H. B., Yang, W., Liu, X. Q., and He, J. Q.: Black soot and the survival of Tibetan glaciers, PNAS, 106, 22114-22118, 2009.
Yang, M., Howell, S. G., Zhuang, J., and Huebert, B. J.: Attribution of aerosol light absorption to black carbon, brown carbon, and dust in China - interpretations of atmospheric measurements during EAST-AIRE, Atmos Chem Phys, 9, 2035-2050, 2009.
Yao, T. D., Thompson, L., Yang, W., Yu, W. S., Gao, Y., Guo, X. J., Yang, X. X., Duan, K. Q., Zhao, H. B., Xu, B. Q., Pu, J. C., Lu, A. X., Xiang, Y., Kattel, D. B., and Joswiak, D.: Different glacier status with atmospheric circulations in Tibetan Plateau and surroundings, Nat. Clim. Change, 2, 663-667, 2012.
Ye, H., Zhang, R., Shi, J., Huang, J., Warren, S. G., and Fu, Q.: Black carbon in seasonal snow across northern Xinjiang in northwestern China, Environ. Res. Lett., 7, 044002, 2012.
You, R., Radney, J. G., Zachariah, M. R., and Zangmeister, C. D.: Measured Wavelength-Dependent Absorption Enhancement of Internally Mixed Black Carbon with Absorbing and Nonabsorbing Materials, Environ. Sci. Technol., 50, 7982-7990, 2016.
Zhang, Y., Kang, S., Cong, Z., Schmale, J., Sprenger, M., Li, C., Yang, W., Gao, T., Sillanpää, M., and Li, X.: Light‐absorbing impurities enhance glacier albedo reduction in the southeastern Tibetan Plateau, J. Geophys. Res.-Atmos., 122, 6915-6933, 2017.
Zhang, Y., Kang, S., Sprenger, M., Cong, Z., Gao, T., Li, C., Tao, S., Li, X., Zhong, X., and Xu, M.: Black carbon and mineral dust in snow cover on the Tibetan Plateau, The Cryosphere, 12, 413-431, 2018.

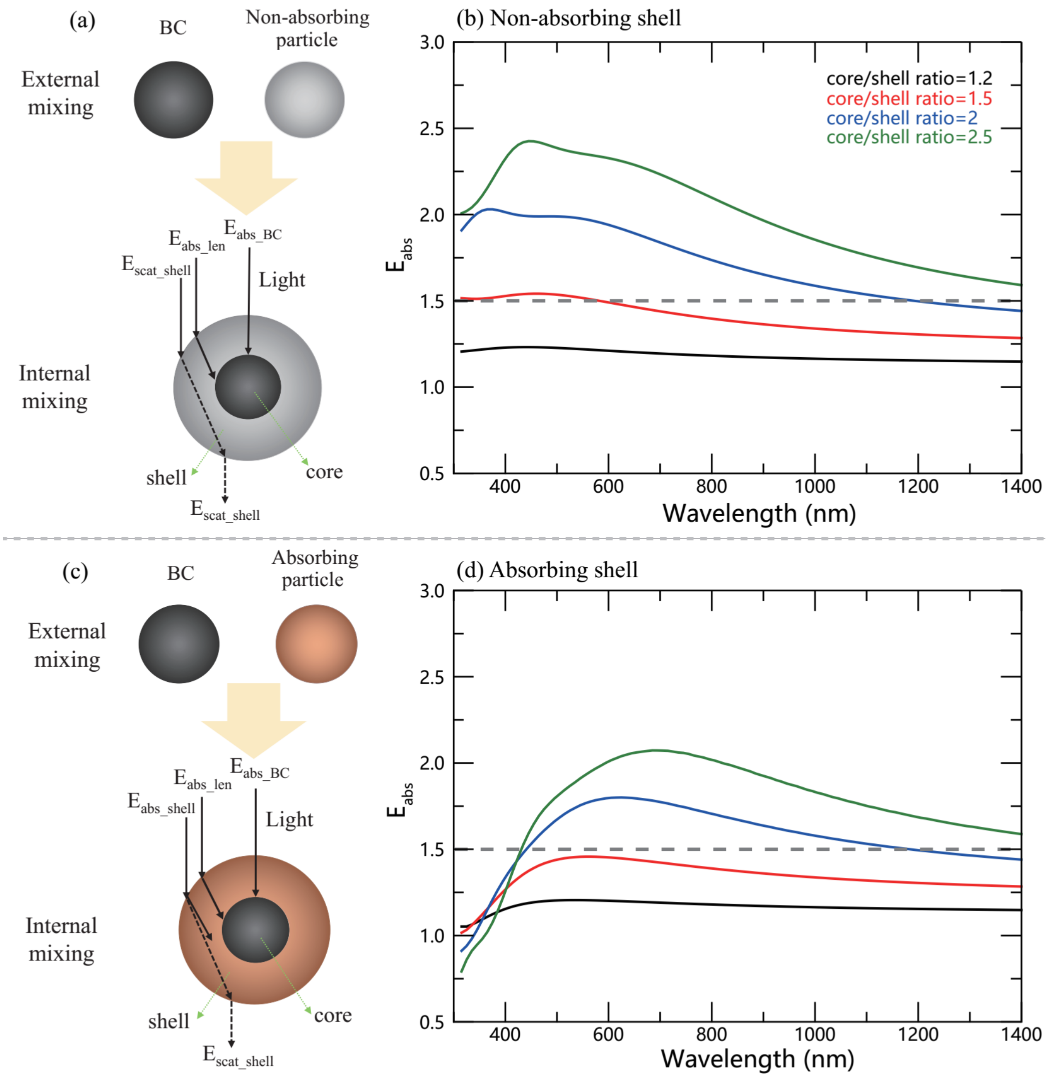

Figure 1. Schematic diagrams showing the light absorption for an external mixture and internal mixture of BC, for (a) a non-absorbing particle and (c) an absorbing particle. Also shown is the enhancement of light absorption from the internal mixture (E_{abs}) compared to the external mixture of BC with (b) non-absorbing and (d) absorbing particles. The internal mixed particle was assumed to be a core/shell structure with a black carbon (BC) core.

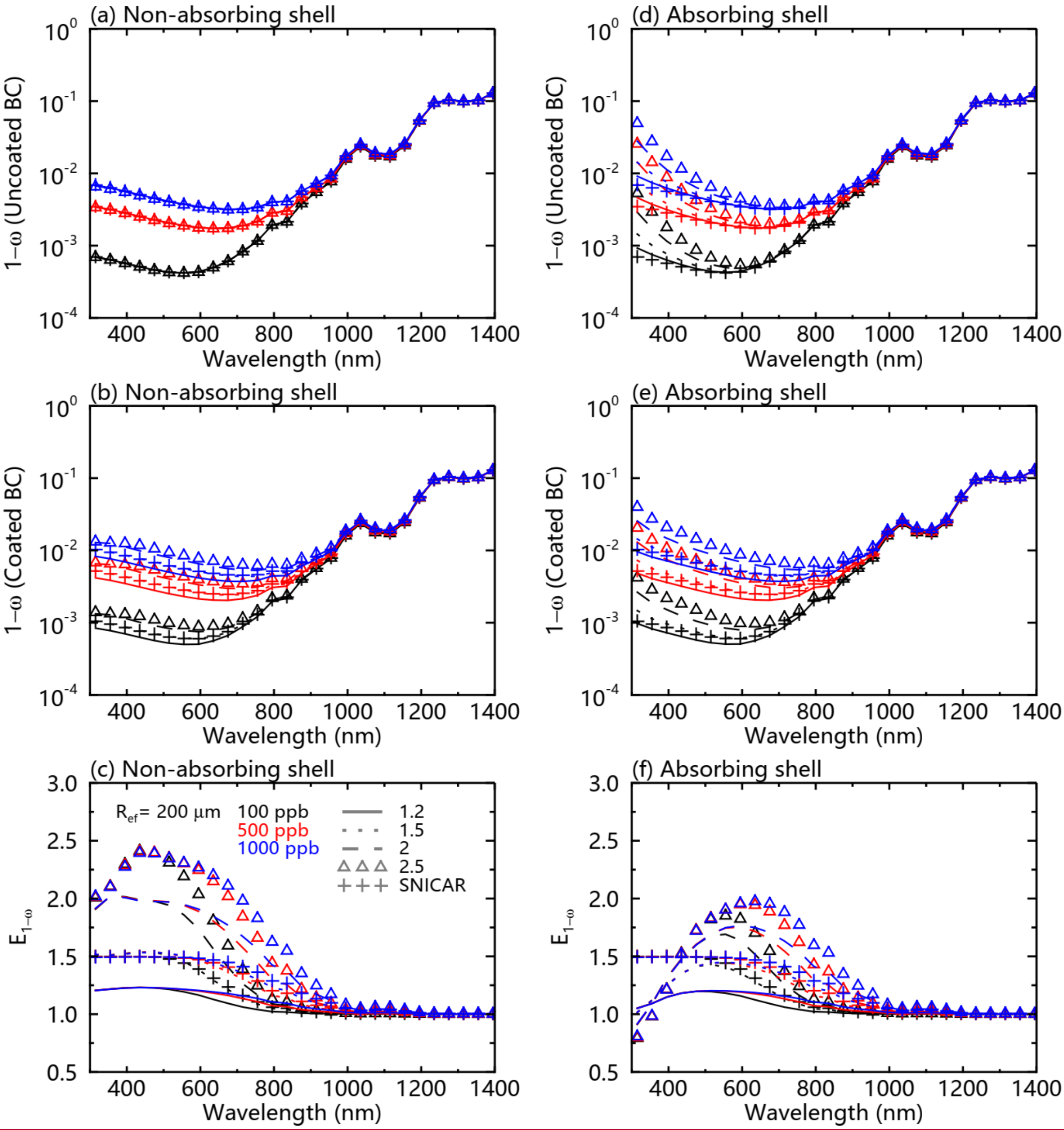

Figure 2. Snow single-scattering co-albedo (1–ω) as a function of wavelength, with different BC concentrations and core/shell ratios for (a) uncoated and (b) coated BC with an assumption of a non-absorbing shell. (d) and (e) are same as (a) and (b), respectively, but with an assumption of an absorbing shell. (c) shows the ratios of snow single-scattering co-albedo ($E_{1-\omega}$) for coated versus uncoated BC with an assumption of a non-absorbing shell. (f) is same as (c), but with an assumption of an absorbing shell. The snow grain radius was assumed to be 200 nm.

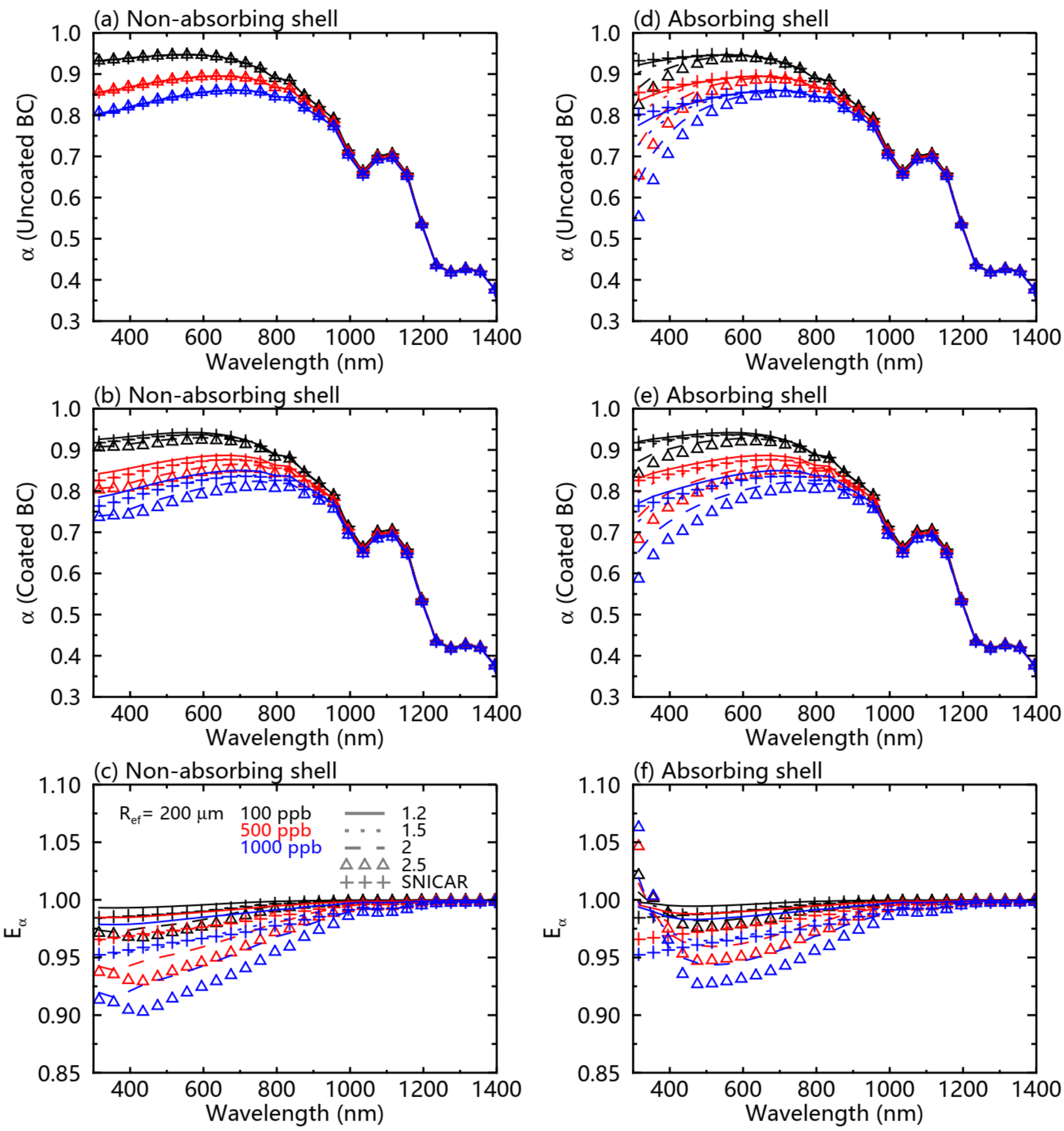

Figure 3. Same as Figure 2, but for snow albedo (α).

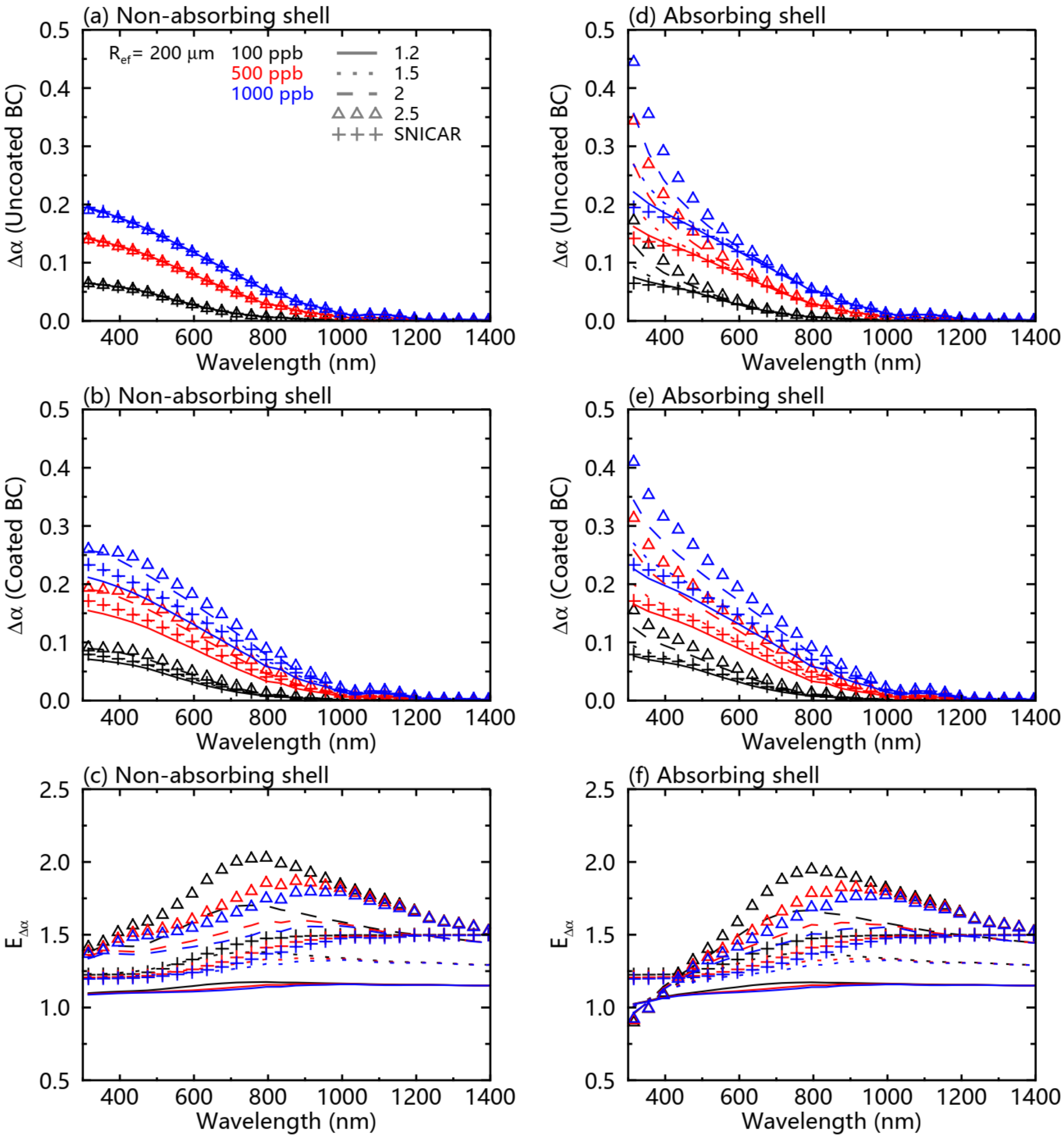

Figure 4. Same as Figure 2, but for snow albedo reduction (Δα).

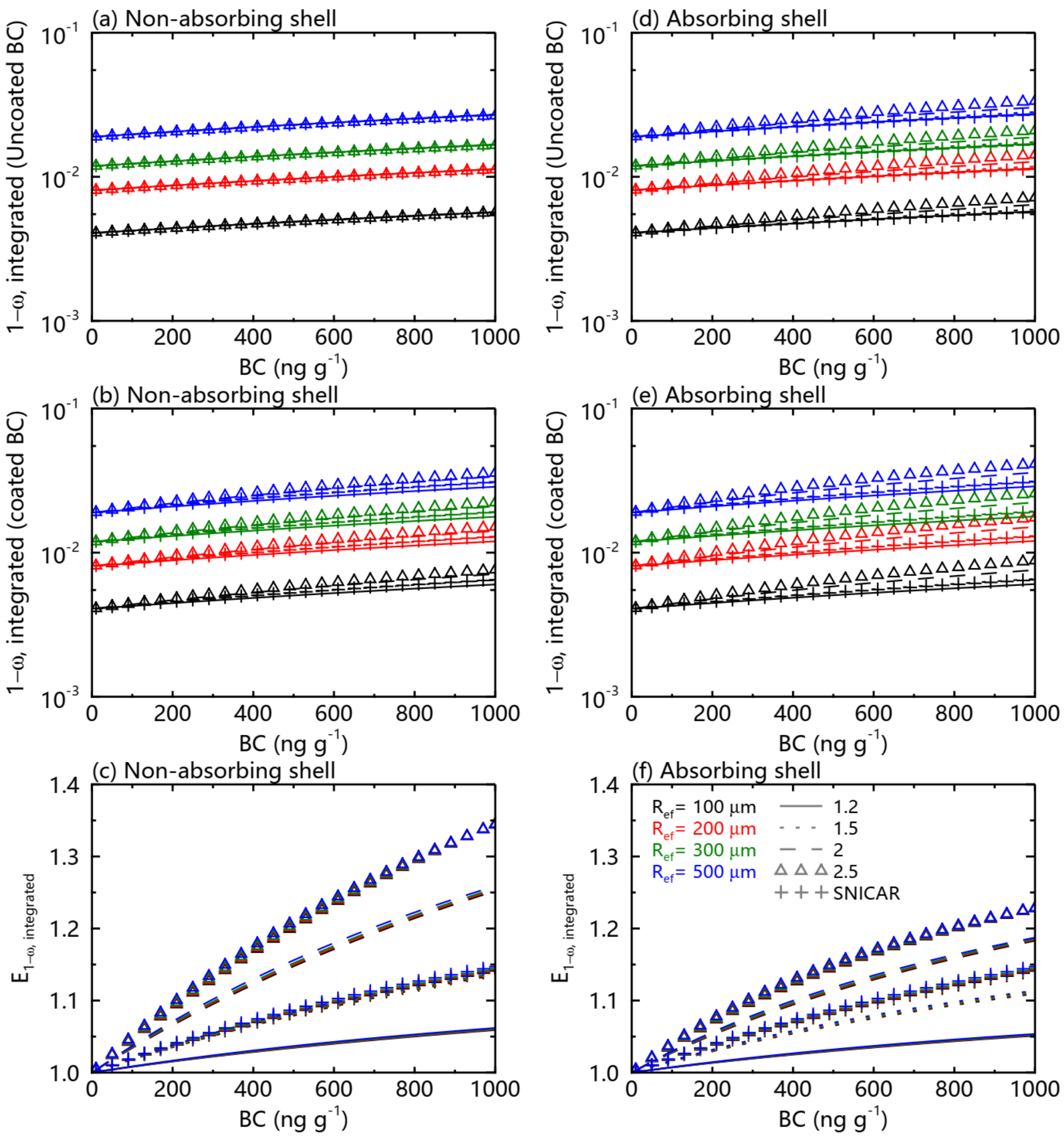

Figure 5. The spectrally weighted snow single-scattering co-albedo (1-$\omega_{integrated}$) over 300–2500 nm of a typical surface solar spectrum at mid–high latitude from January to May, for (a) uncoated and (b) coated BC with an assumption of a non-absorbing shell. (d) and (e) are same as (a) and (b), respectively, but with an assumption of an absorbing shell. (c) shows the ratios ($E_{1-\omega,\ integrated}$) of spectrally weighted snow single-scattering co-albedo for coated versus uncoated BC with an assumption of a non-absorbing shell. (f) is same as (c), but with an assumption of an absorbing shell.

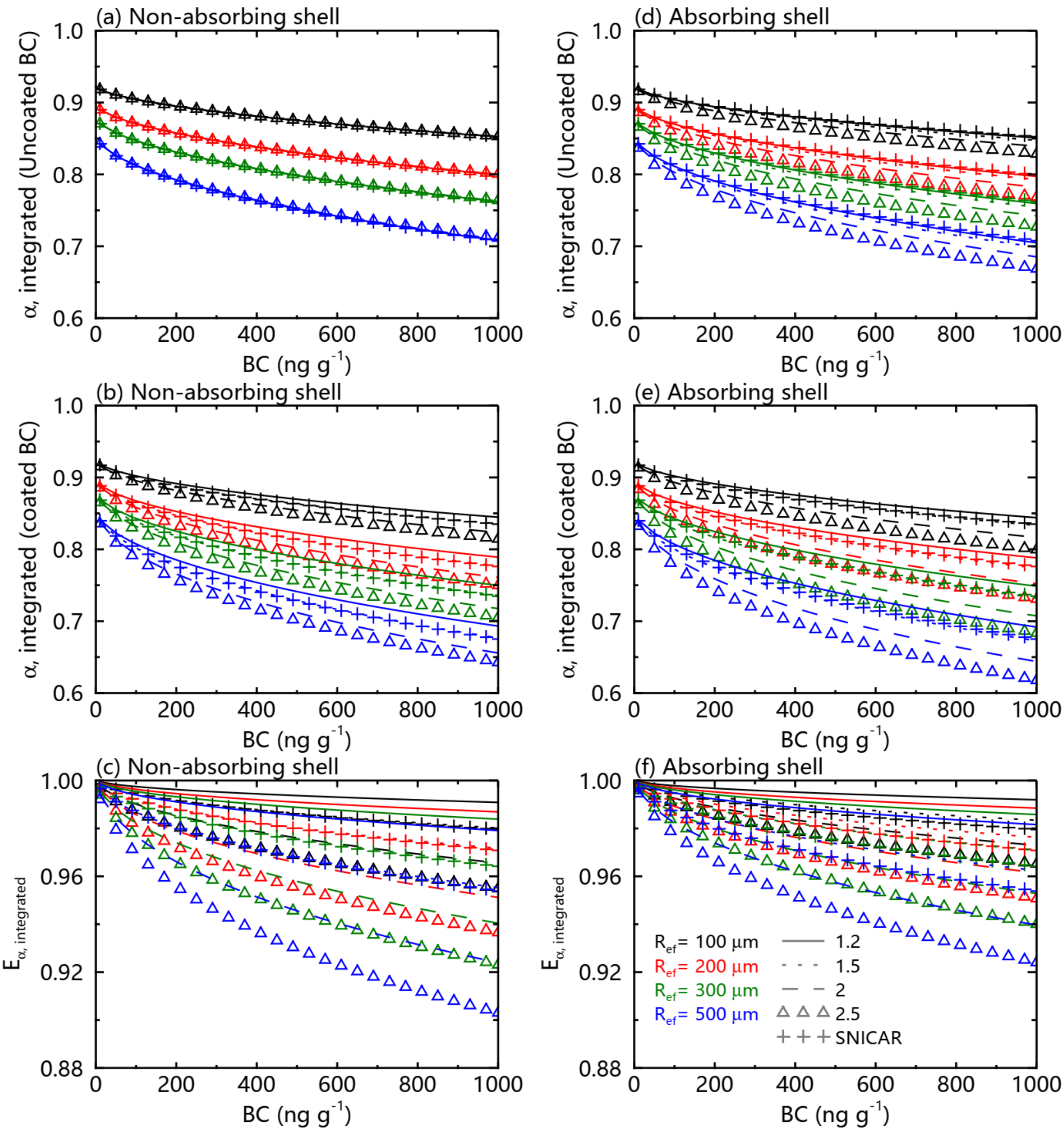

Figure 6. Same as Figure 5, but for snow albedo ($\alpha_{integrated}$).

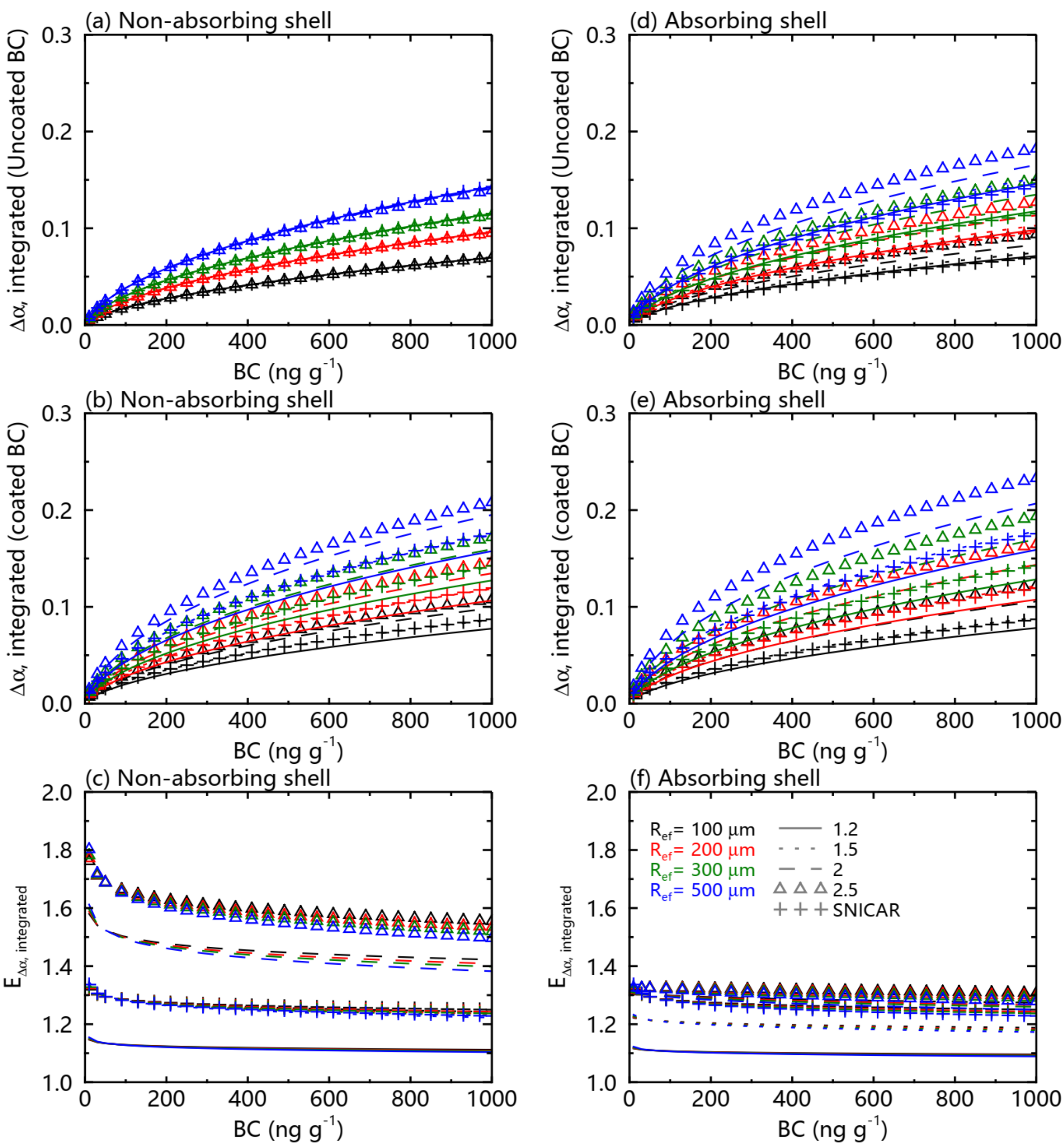

Figure 7. Same as Figure 5, but for snow albedo reduction ($\Delta\alpha_{integrated}$).

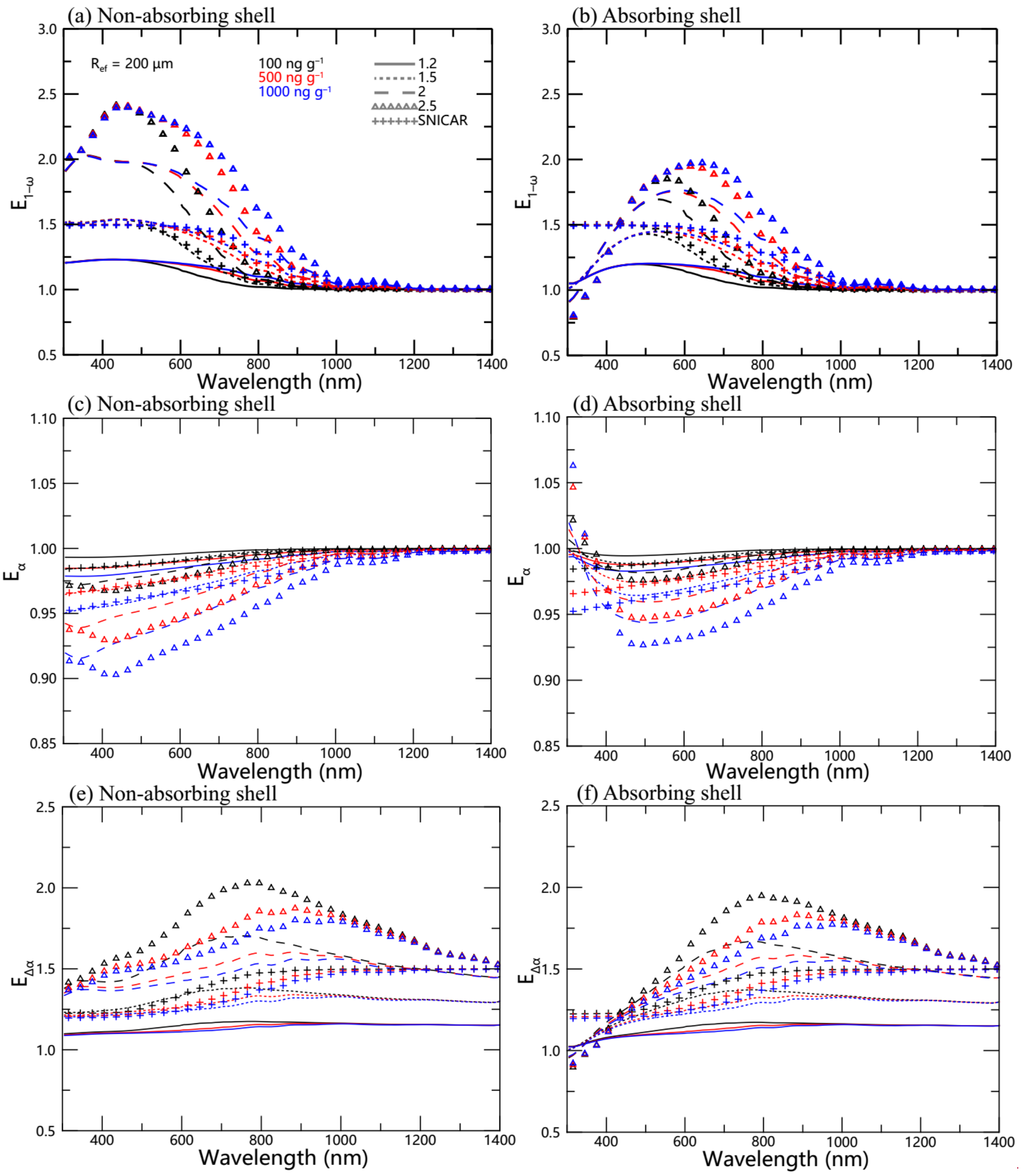

Figure 2. Ratios of snow single-scattering co-albedo ($E_{1-\omega}$) from an internal mixed particle to an external mixed particle as a function of wavelength, with different BC concentrations and core/shell ratios for (a) a non-absorbing shell, and (b) an absorbing shell. (c) and (d) Same as (a) and (b), but for snow albedo (E_{α}). (e) and (f) Same as (a) and (b), but for snow albedo reduction ($E_{\Delta\alpha}$). The snow grain radius was assumed to be 200 nm.

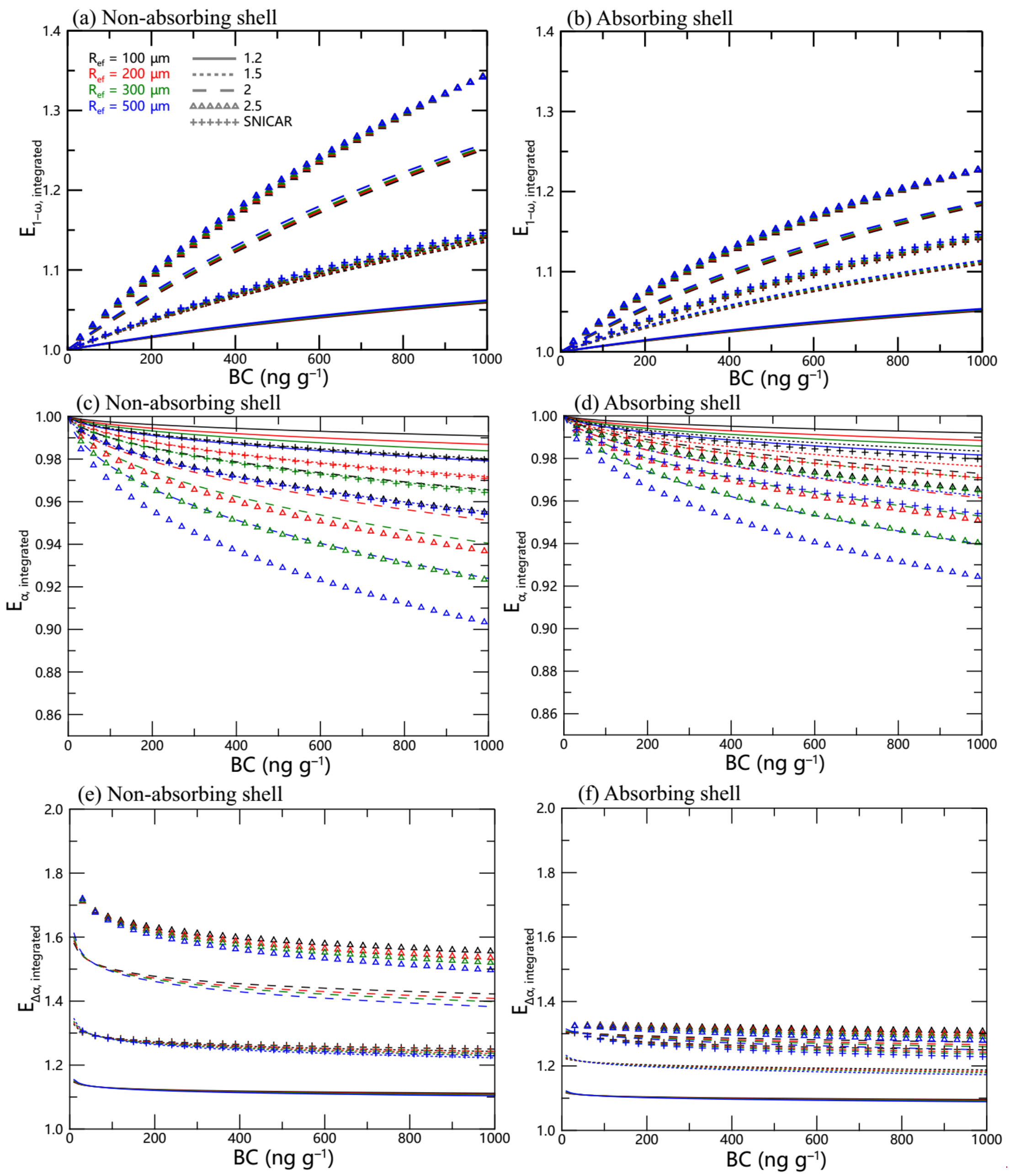

Figure 3. The spectrally weighted $E_{1-\omega}$ ($E_{1-\omega,\ integrated}$) over 300–1400 nm of a typical surface solar spectrum at mid-high latitude from January to May, for (a) a non-absorbing shell and (b) an absorbing shell as a function of black carbon (BC) concentration with different snow grain radii and core/shell ratios. (c) and (d) Same as (a) and (b), but for broadband snow albedo ($E_{\alpha,\ integrated}$). (e) and (f) Same as (a) and (b), but for broadband snow albedo reduction ($E_{\Delta\alpha,\ integrated}$).

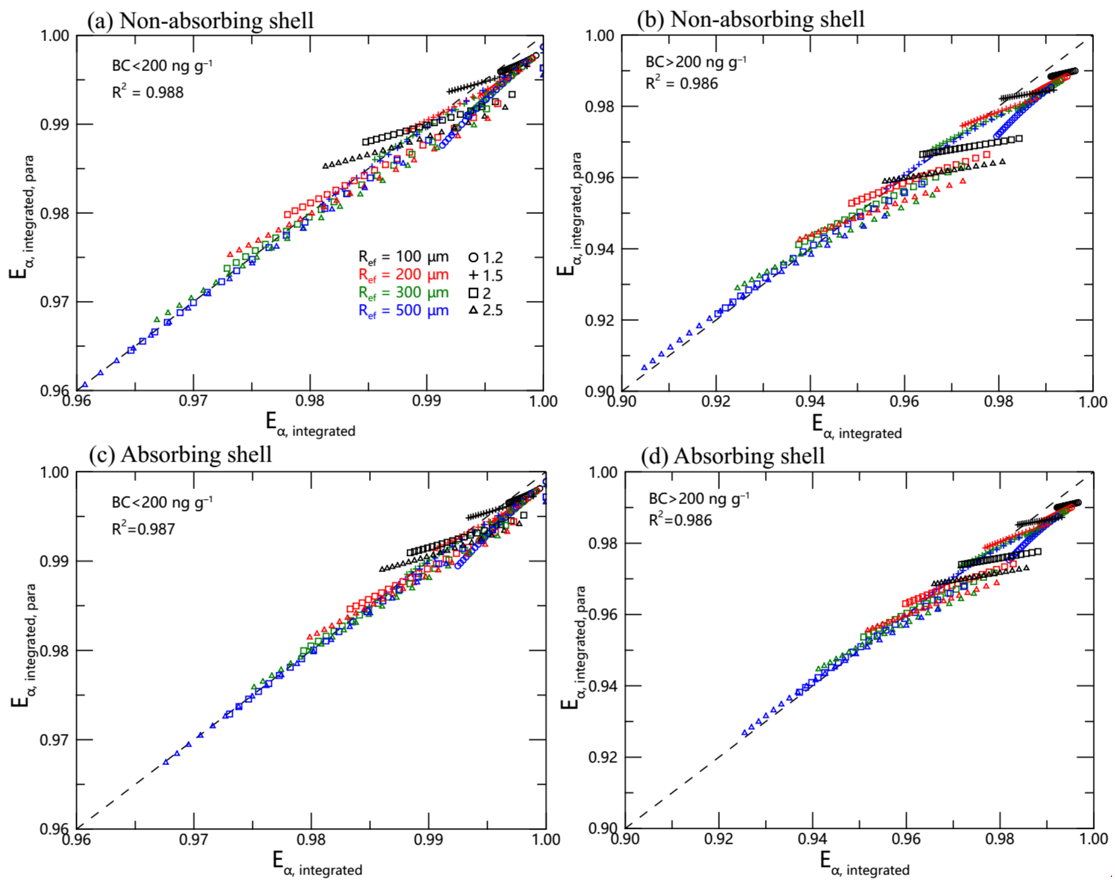

(a) Non-absorbing shell
BC<200 ng g⁻¹
R^2 = 0.988
R_{ef} = 100 μm ○ 1.2
R_{ef} = 200 μm + 1.5
R_{ef} = 300 μm □ 2
R_{ef} = 500 μm △ 2.5
$E_{\alpha, integrated, para}$
$E_{\alpha, integrated}$
(b) Non-absorbing shell
BC>200 ng g⁻¹
R^2 = 0.986
(c) Absorbing shell
BC<200 ng g⁻¹
R^2=0.987
(d) Absorbing shell
BC>200 ng g⁻¹
R^2=0.986

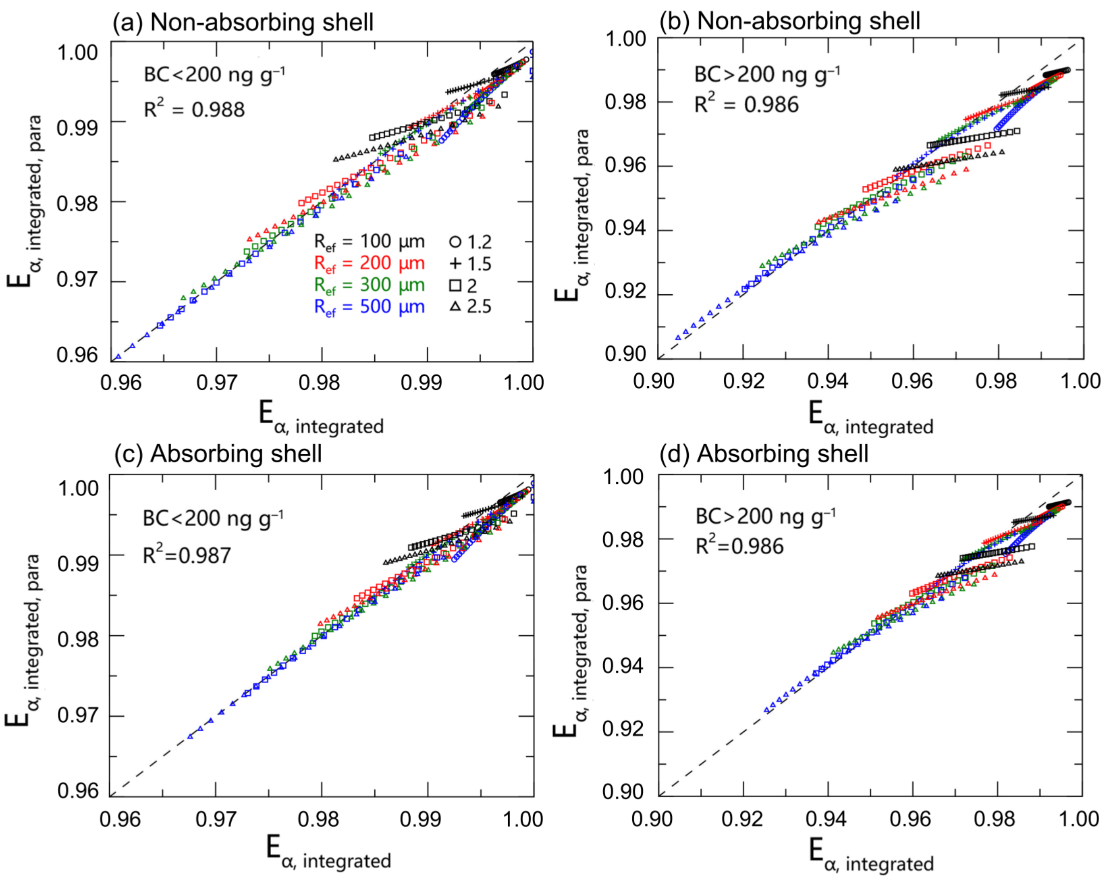

(a) Non-absorbing shell
BC<200 ng g⁻¹
R^2 = 0.988
R_{ef} = 100 μm ○ 1.2
R_{ef} = 200 μm + 1.5
R_{ef} = 300 μm □ 2
R_{ef} = 500 μm △ 2.5
$E_{\alpha, integrated, para}$
$E_{\alpha, integrated}$
(b) Non-absorbing shell
BC>200 ng g⁻¹
R^2 = 0.986
(c) Absorbing shell
BC<200 ng g⁻¹
R^2=0.987
(d) Absorbing shell
BC>200 ng g⁻¹
R^2=0.986

Figure 84. Comparisons of model calculated $E_{\alpha,\ integrated}$ and parameterized $E_{\alpha,\ integrated,\ para}$ for (a) relatively clean snow (BC concentration <1000 200 ng g^{-1}), and (b) relatively polluted snow (BC concentration >1000 200 ng g^{-1}) for a non-absorbing shell. (c) and (d) Same as (a) and (b), but for an absorbing shell.

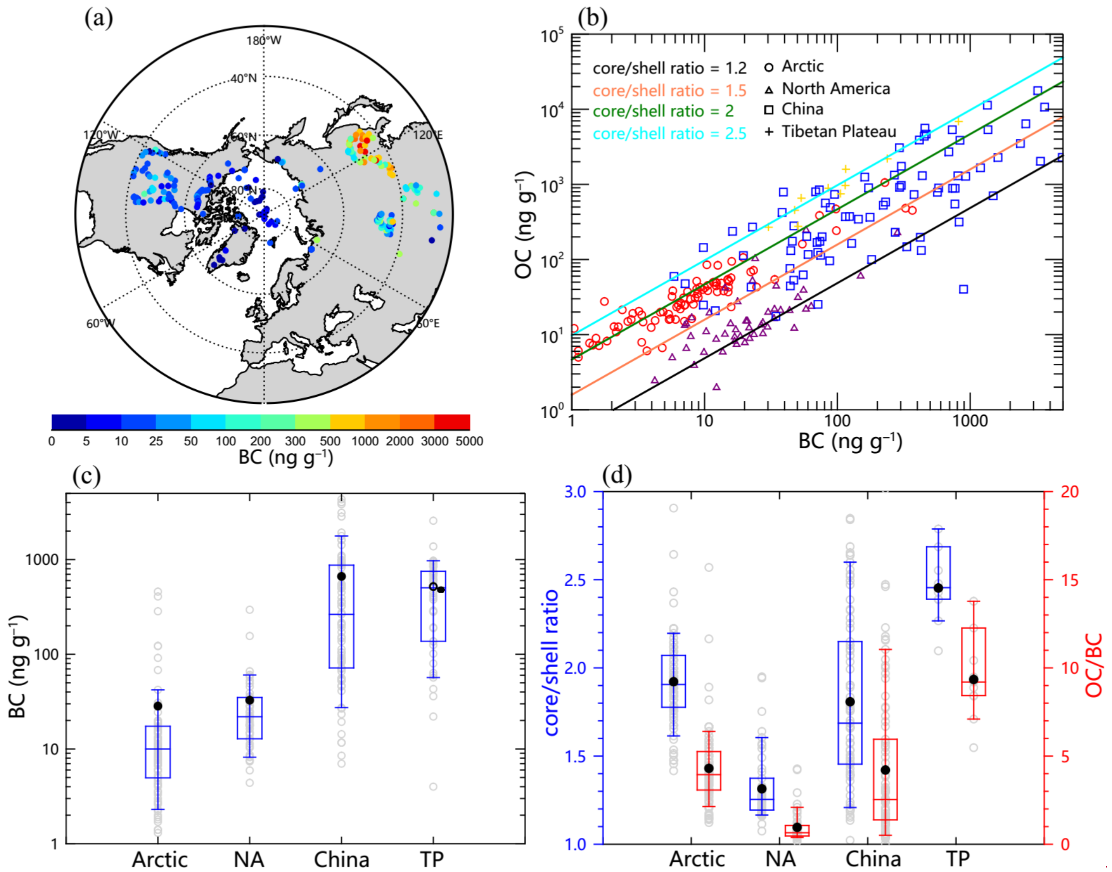

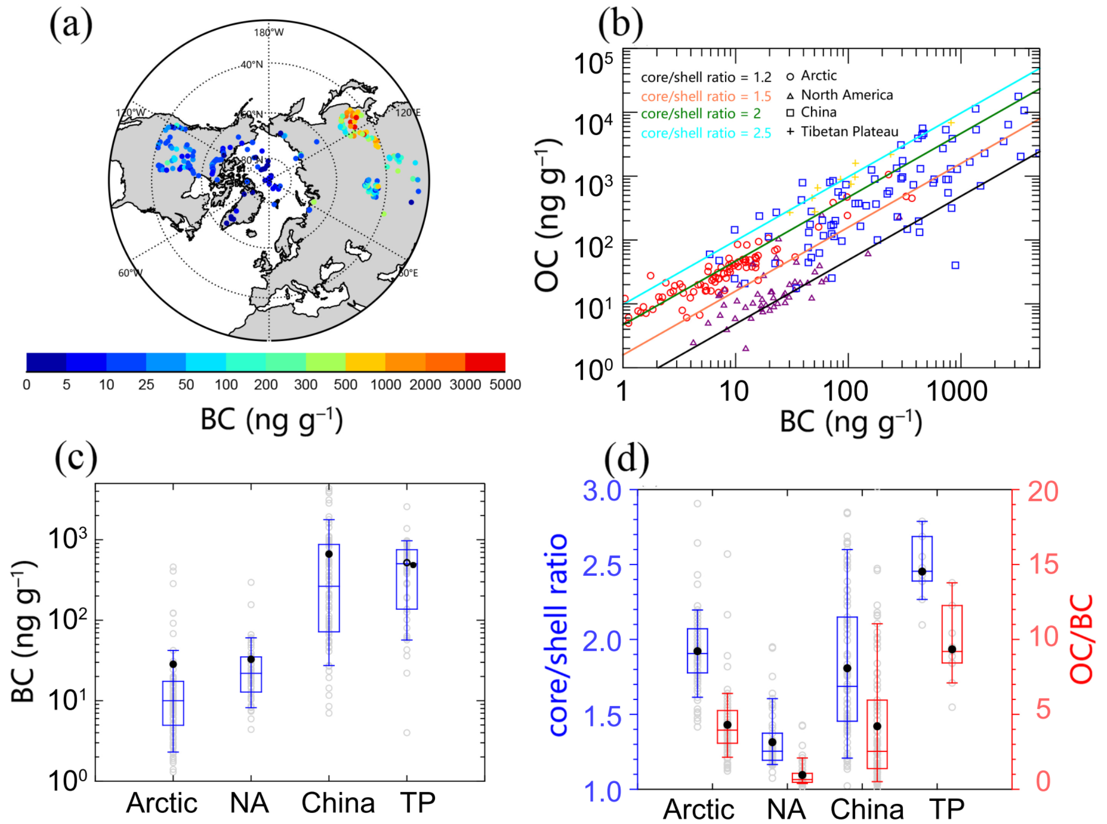

Figure 95. (a) The spatial distribution of measured black carbon (BC) concentrations

across the Northern Hemisphere. (b) Comparison of BC and organic carbon (OC) concentrations in: the Arctic, North America (NA), northern China (NC) and the Tibetan Plateau (TP). (c) Statistical plots of BC concentrations in different regions. The boxes denote the 25th and 75th quantiles, the horizontal lines denote the 50th quantiles (medians), solid dots denote averages, and whiskers denote the 10th and 90th quantiles. In situ data is shown as gray circles. (d) Same as (c) but for a core/shell ratio and OC/BC mass ratio, assuming a core/shell structure with a BC core and an absorbing OC shell.

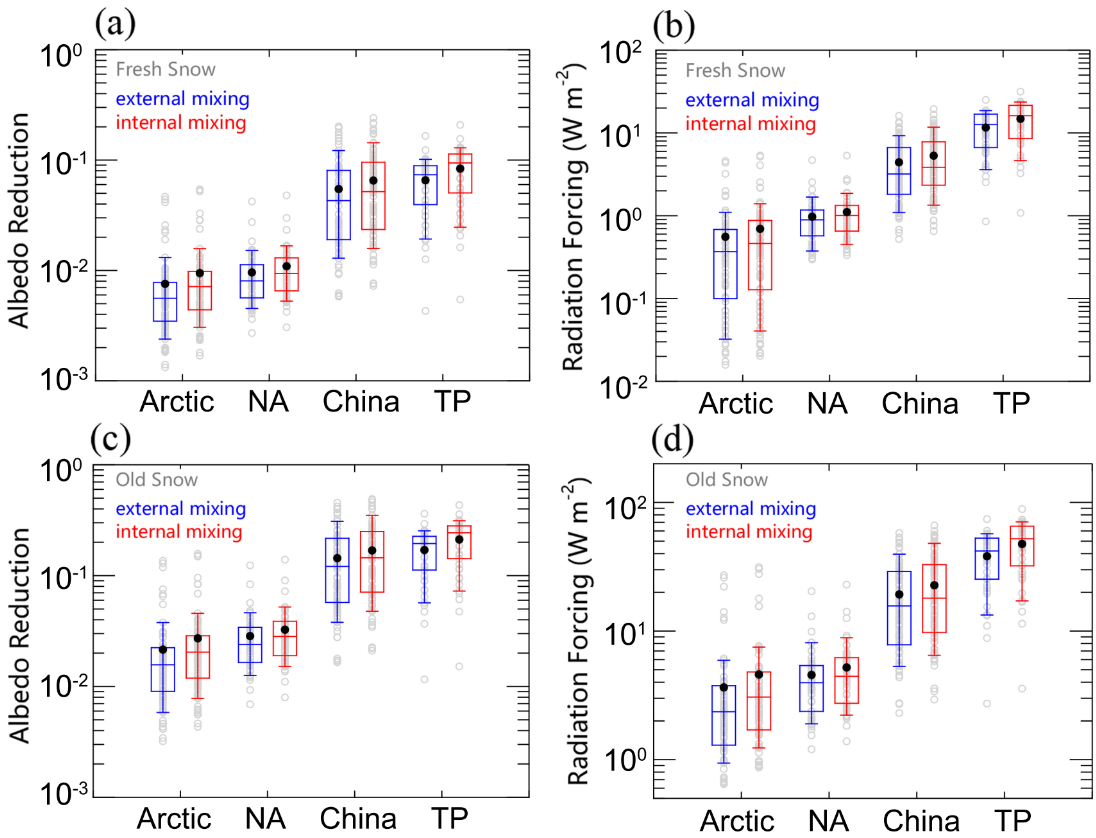

Figure 10. Statistical plots of (a) albedo reduction, and (b) radiative forcing, in different regions for fresh snow. (c) and (d) Same as (a) and (b), but for old snow. The boxes denote the 25th and 75th quantiles, horizontal lines denote the 50th quantiles (medians), solid dots denote averages, and whiskers denote the 10th and 90th quantiles. In situ data is shown as gray circles.

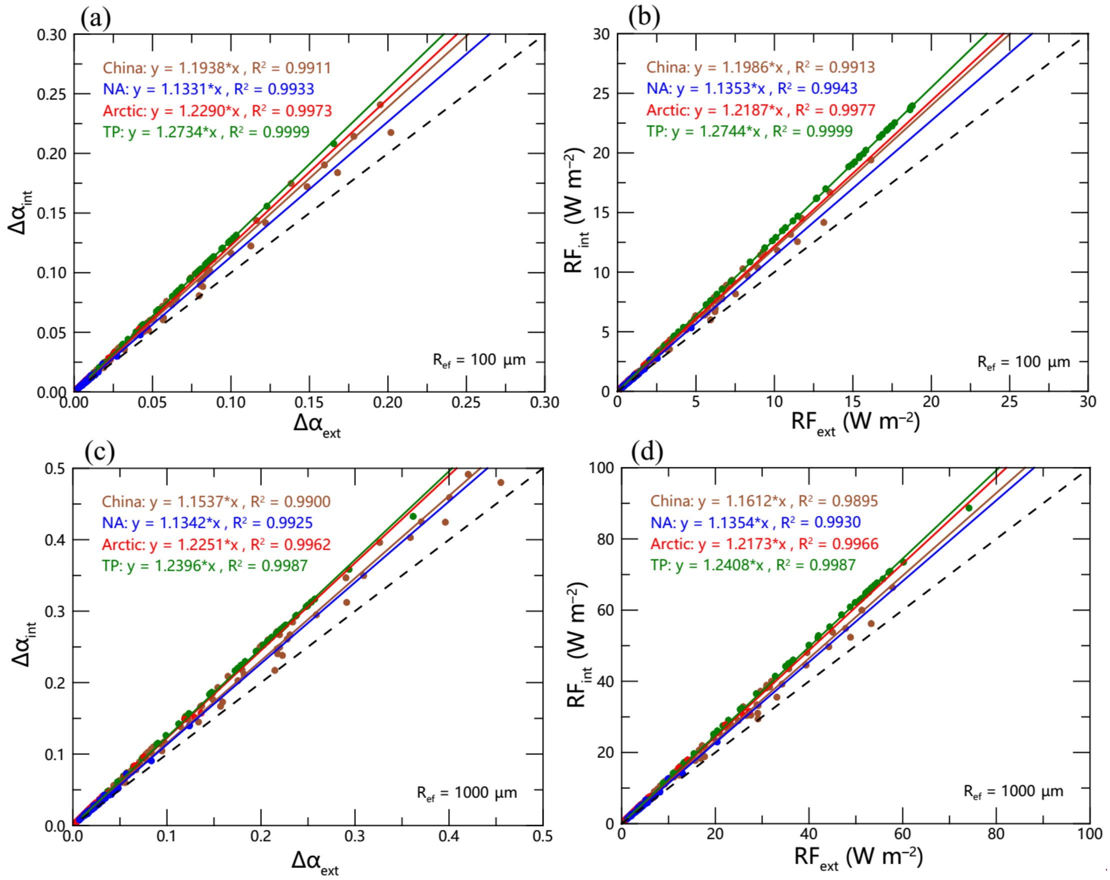
(a)
China: y = 1.1938*x , R² = 0.9911
NA: y = 1.1331*x , R² = 0.9933
Arctic: y = 1.2290*x , R² = 0.9973
TP: y = 1.2734*x , R² = 0.9999
Δα_int
Δα_ext
R_ef = 100 μm
(b)
China: y = 1.1986*x , R² = 0.9913
NA: y = 1.1353*x , R² = 0.9943
Arctic: y = 1.2187*x , R² = 0.9977
TP: y = 1.2744*x , R² = 0.9999
RF_int (W m⁻²)
RF_ext (W m⁻²)
R_ef = 100 μm
(c)
China: y = 1.1537*x , R² = 0.9900
NA: y = 1.1342*x , R² = 0.9925
Arctic: y = 1.2251*x , R² = 0.9962
TP: y = 1.2396*x , R² = 0.9987
Δα_int
Δα_ext
R_ef = 1000 μm
(d)
China: y = 1.1612*x , R² = 0.9895
NA: y = 1.1354*x , R² = 0.9930
Arctic: y = 1.2173*x , R² = 0.9966
TP: y = 1.2408*x , R² = 0.9987
RF_int (W m⁻²)
RF_ext (W m⁻²)
R_ef = 1000 μm

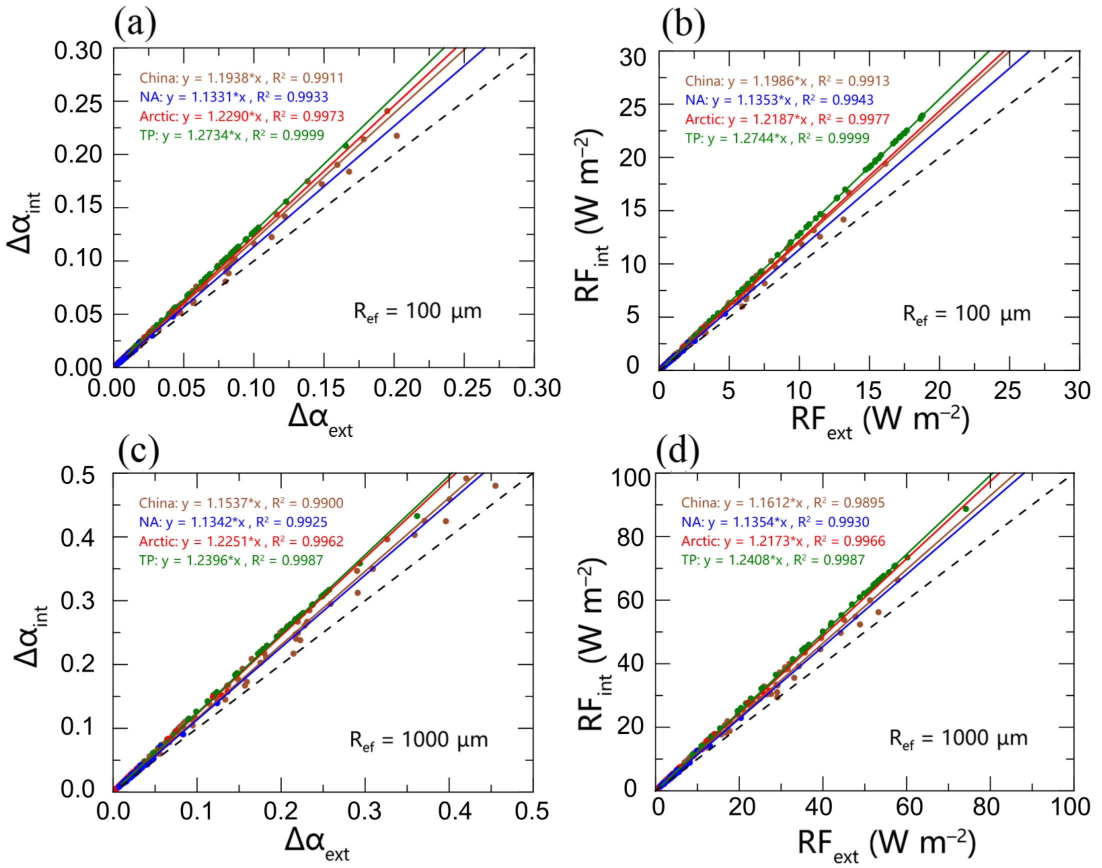

Figure 116. Comparisons of (a) the snow albedo reduction and (b) the radiative forcing by an internal mixed particle versus an external mixed particle, based on in situ measurements of fresh snow (assuming a snow grain radius of 100 μm). (c) and (d) Same as (a) and (b), but for old snow and assuming a snow grain radius of 1000 μm.

1